With the shielding system the values of magnetic flux density is reduced as shown in Figure 91
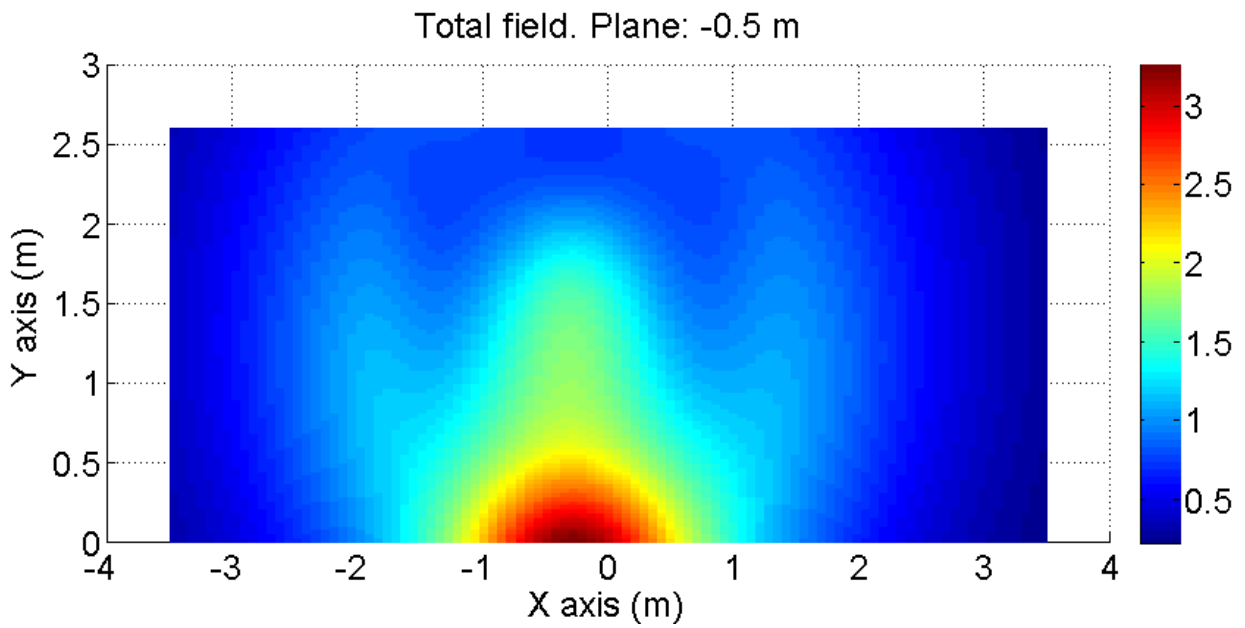

Figure 91 Field map in μT of the computed values of magnetic induction generated by the MV switchgear on a x-z (with y equal to −0.5 m) plane after the positioning of the shielding system

The values of shielding factor achieved with the installation of the shield are presented in Figure 92
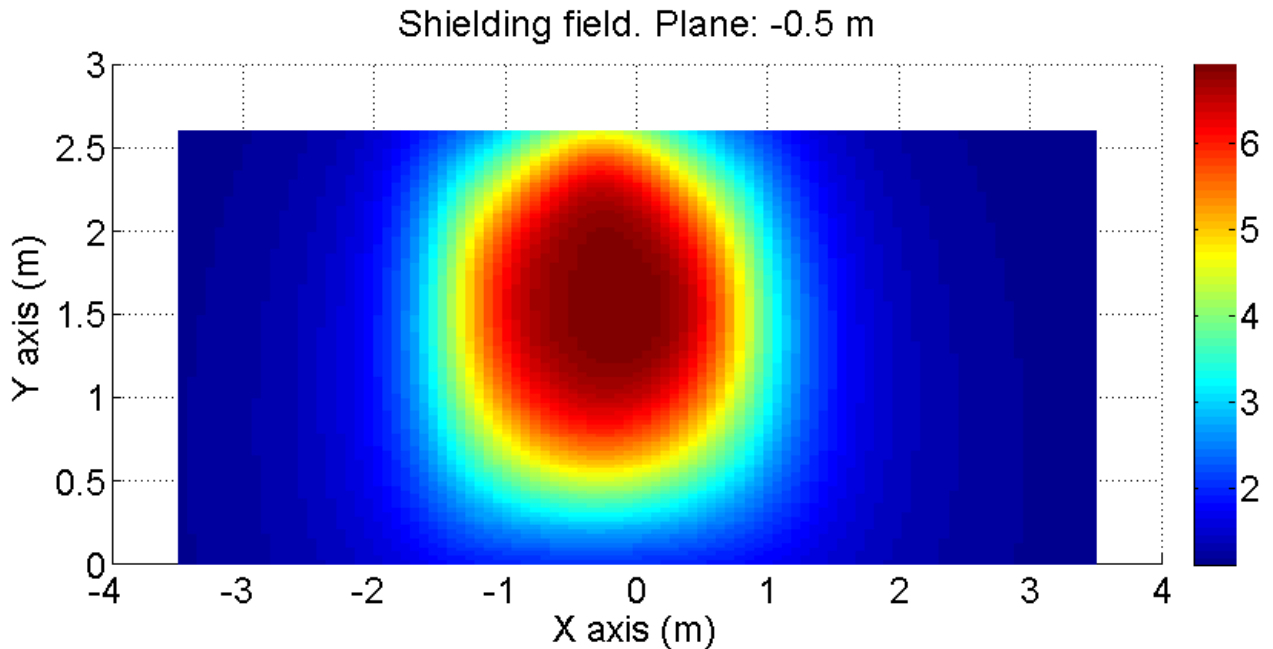

Figure 92 Field map of the SF achieved with the installation of the shielding system

The shielding system designed for this application provides a significant reduction of the values of magnetic induction but, due to the high end effect, at heights closer to the ground the values of magnetic induction are slightly lower than the prefixed limit.

➢ LV Switchgear

Even for the LV switchgear the analysis can be carried out taking in account only an x-z plane. The position of the computation planes relative to the shield is reported in Figure 93.
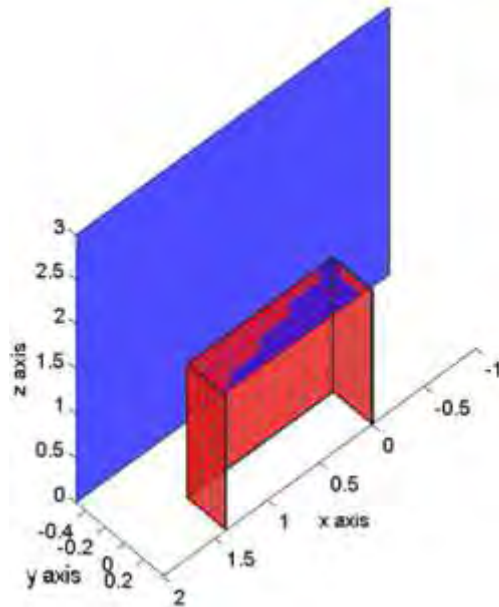

Figure 93 Layout of the shielding system (in red) with the computation planes (in blue)

The computation of the values of magnetic induction generate by the MV switchgear, without the shielding system, is presented in Figure 94
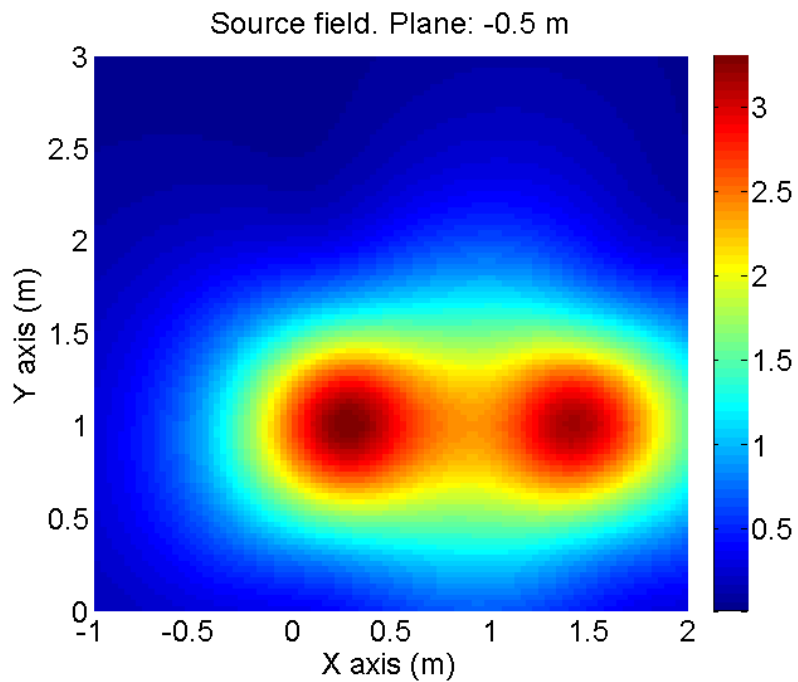

Source field. Plane: -0.5 m

Figure 94 Field map in µT of the computed values of magnetic induction generated by the LV switchgears on a x-z plane

With the shielding system the values of magnetic flux density is reduced as shown in Figure 95
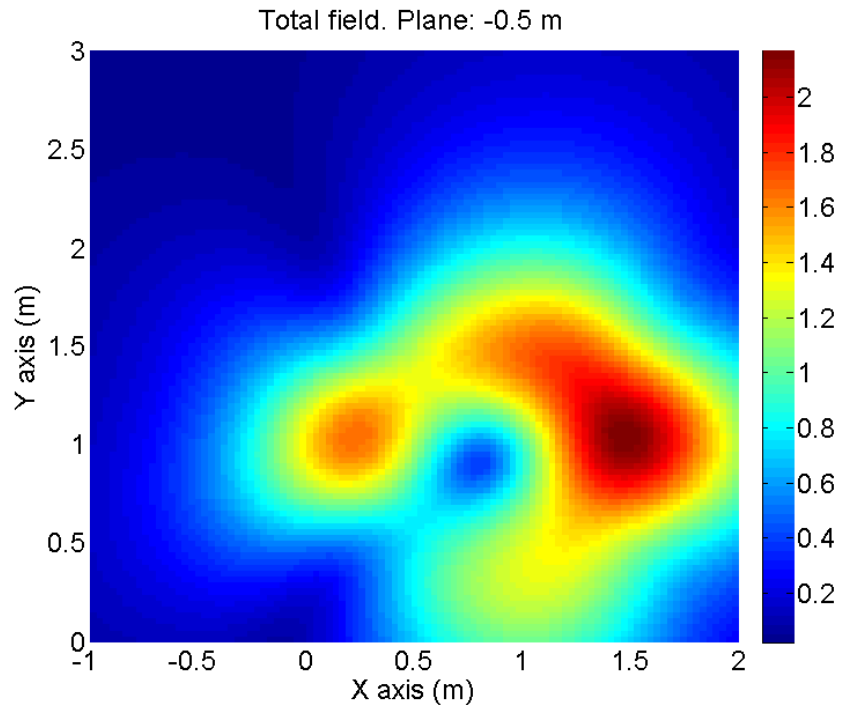

Total field. Plane: -0.5 m

Figure 95 Field map in µT of the computed values of magnetic induction generated by the LV switchgear on a x-z (with y equal to −0.5 m) plane after the positioning of the shielding system

The values of shielding factor achieved with the installation of the shield are presented in Figure 96
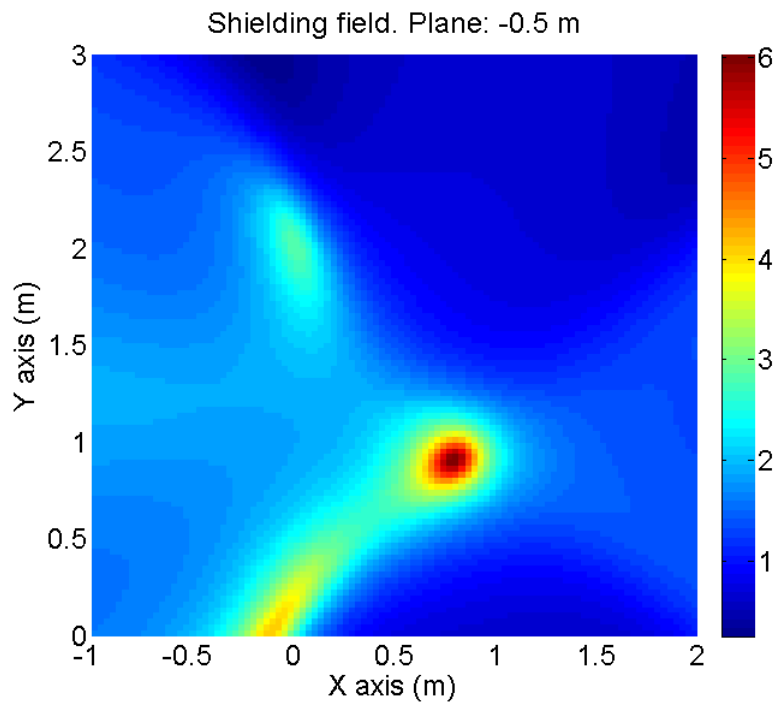

Shielding field. Plane: -0.5 m

Figure 96 Field map of the SF achieved with the installation of the shielding system

The shielding factor provided with this shielding solution is relatively low but enough to reach the goal set.

In the three different shielding system described in this subsection the shielding appendix are the key to reach the goal set. In fact the shielding system design for a single device is relatively small and therefore the currents reclosing at the edges are high and this results in a bigger end-effect. The shielding appendix move, in part, this effect within the MV/LV substation where generate a negligible influence.

➢ LV power lines

The LV power lines, being crossed by the all LV current of the transformer (909 A), if is not arranged in the correct way generate high value of magnetic induction as show in Figure 97.
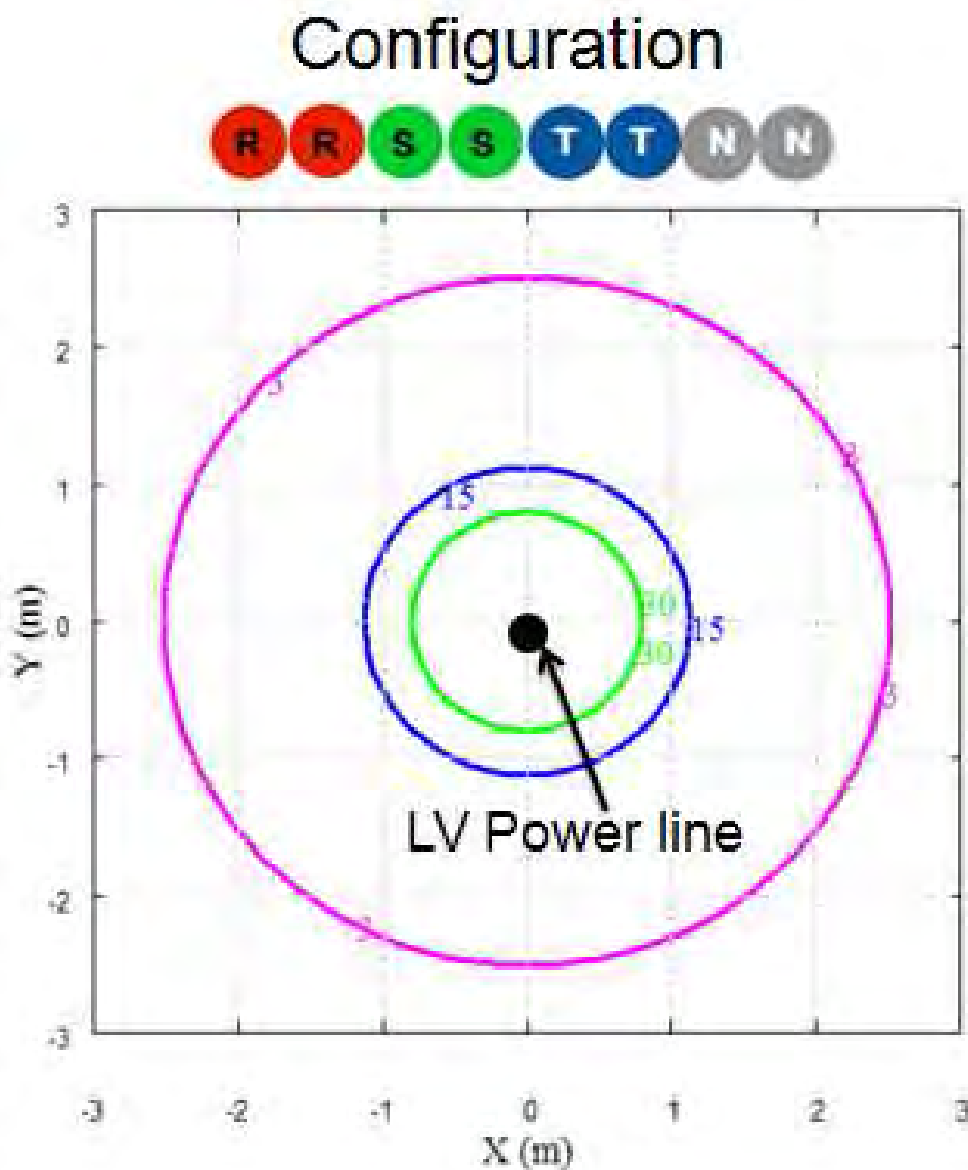

Figure 97 Isolevel lines relative at the value of magnetic induction generate by a power line arranged as show on the top of the figure and crossed by 909 A.

In this case for the attenuation of the values of magnetic induction is not necessary to design a specific shielding system but is enough to arrange the sub conductor of the line in a correct way. For this application the best configuration and the results obtain with it are presented in Figure 98
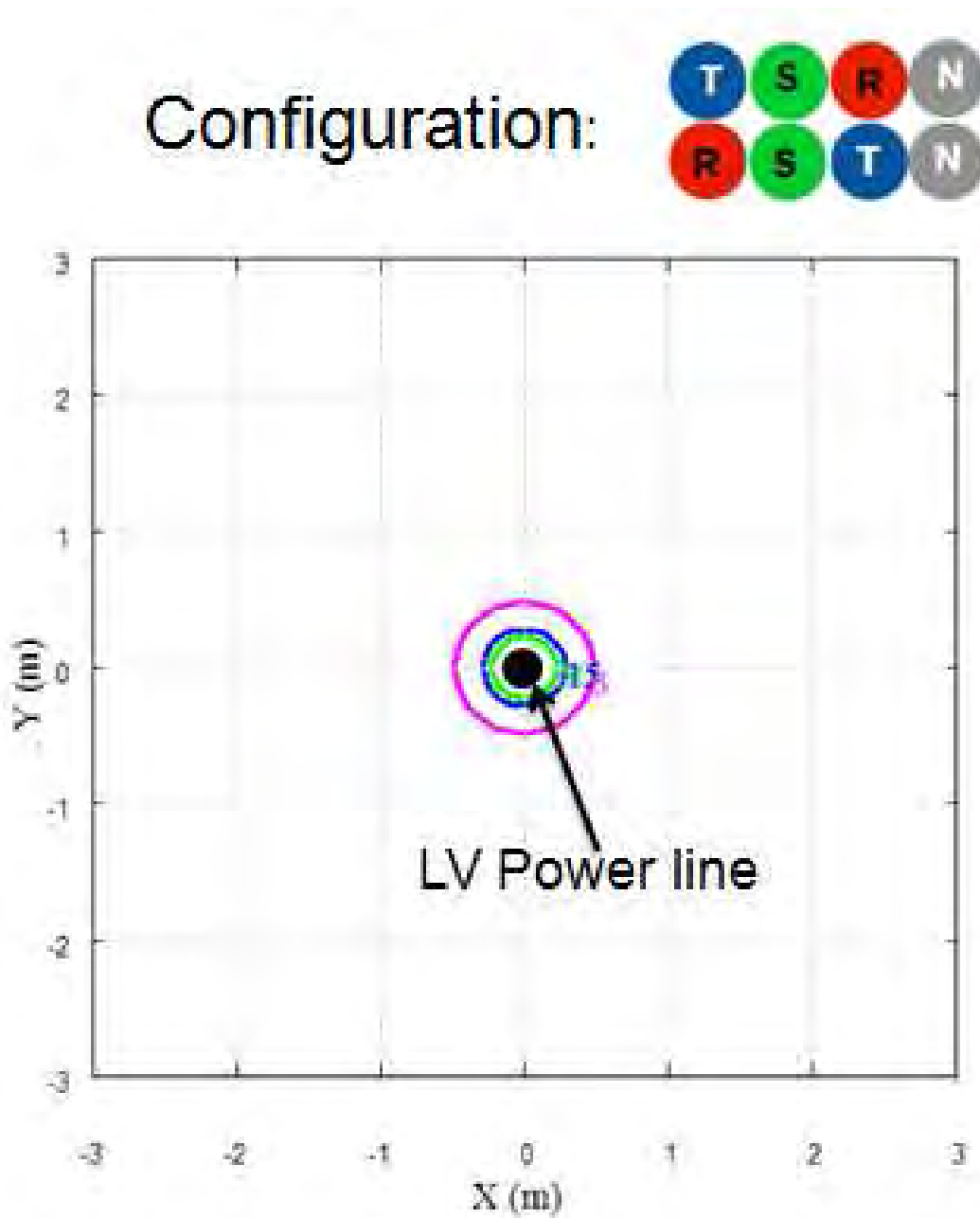
4.4.5   Implementation of the shielding system

In order to verify in a real case that the goal is reached and understand the possible application problems the shielding systems have been produced and installed in a real MV/LV substation of the local distributor. The image of the three shielding system are presented respectively in Figure 99 (a) for the transformer, in Figure 99 (b) for the MV switchgear and in Figure 99 (c) for the three LV switchgears.

Figure 99 Image of the shielding system of the: Transformer (a); MV Switchgear (b); LV Switchgears (c).

4.4.6   Real test of the shielding system and conclusion

After the installation of the devices the MV/LV substation has been inserted in medium voltage ring and commissioning. The test of the shield has been carried out making the measurements of the values of magnetic induction all around the MV/LV substation. The measurements have been made with a special probe regularly calibrate. Every 50 cm of the perimeter of the substation three measures, at different distance(30 cm; 50 cm and 1 m) from the external wall of the substation, have been carried out. The measurements have been made on a x-y plane parallel at the floor of the substation and positioned at an height z equal to 1 m. Being the values of magnetic induction directly proportional to the current that generate it, the current of the MV ring and of the low voltage output of the transformer have been measured and saved every fifteen seconds in order to refer each measure of the magnetic induction respectively at the rated current of the MV ring and of the transformer. The layout of the measurement point are shown in Figure 100 In the same figure are highlighted, using a red color, the points where the goal was not reached.
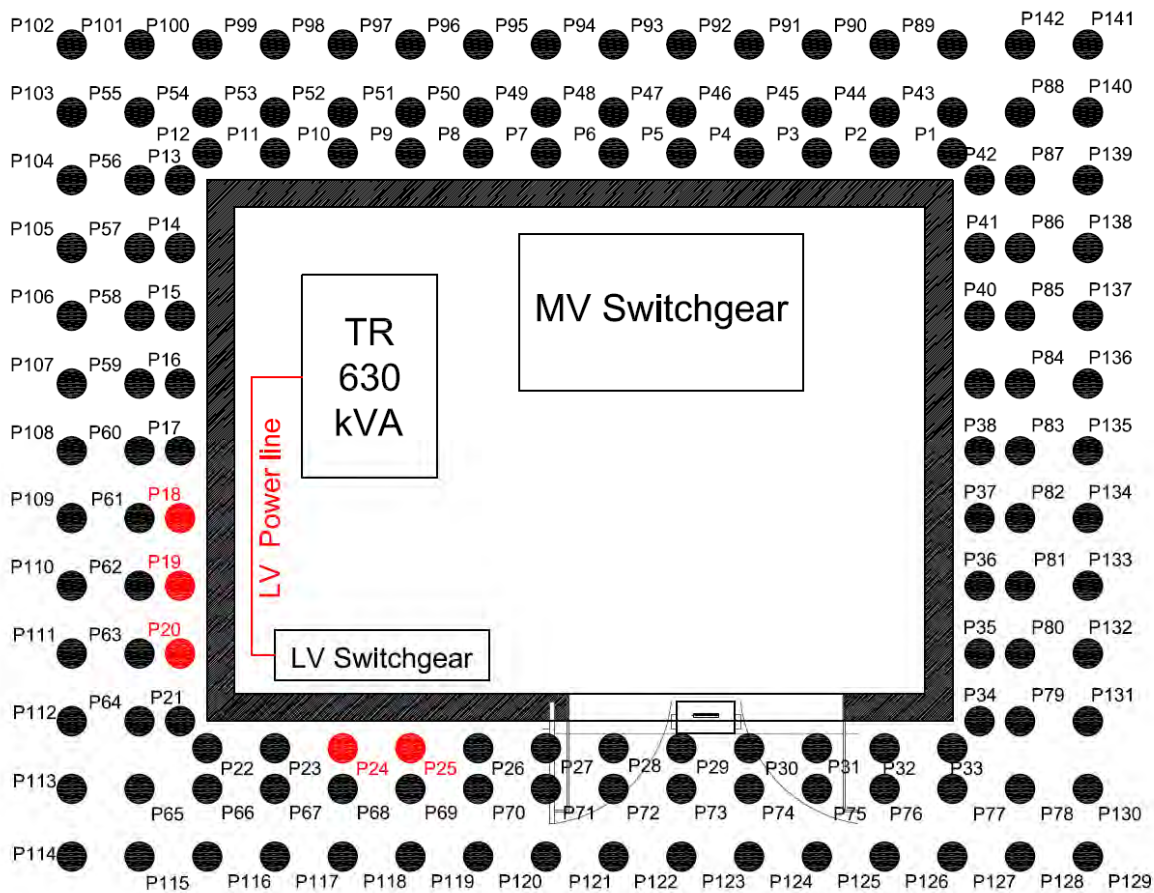

Figure 100 Layout of the measuring points with highlighted in red the points were the goal is not reached

As shown in Figure 100 in five points the goal is not reached. In particular the critical points are in correspondence of the LV power lines and of the LV switchgears. After a careful analysis it was determined the reason for the failure to achieve the objective. The difference from the computed and measured values are due to the LV neutral current that reduces the natural partial cancellation of the fields produced by the three different phases.

Comprised the reason of the difference between the simulated and measured values we have chosen to take action by implementing a configuration of the LV line that takes account of the mismatch between the three different phases and an implementation, with the addition of a lower and an upper appendix, to shielding system of the LV switchgears.

With the previous configuration of the LV power lines, in case of mismatch of the 20% on a single phase, the values of magnetic induction generated by the line rise up as show in Figure 101
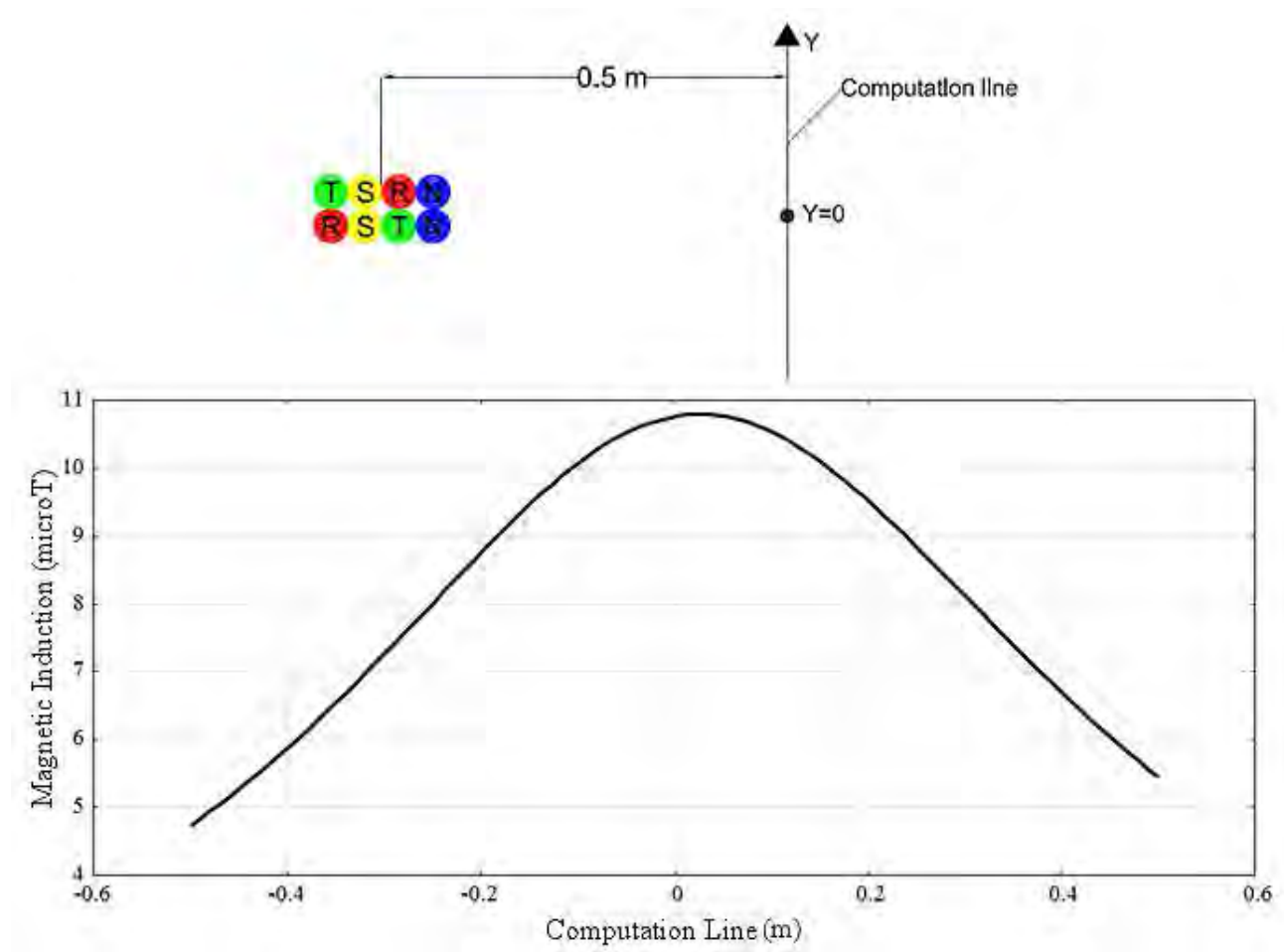

Figure 101 Magnetic induction generate by a LV power lines crossed by a current of 909 A with a mismatch on a single phase equal to 200 A, the configuration of the line is show in upper part of the figure.

In case of mismatch it is therefore recommend to change the arrangement of the phases in order to bring the neutral close as possible to the barycentre of the line. A possible configuration and the results obtained with it are presented in Figure 102.
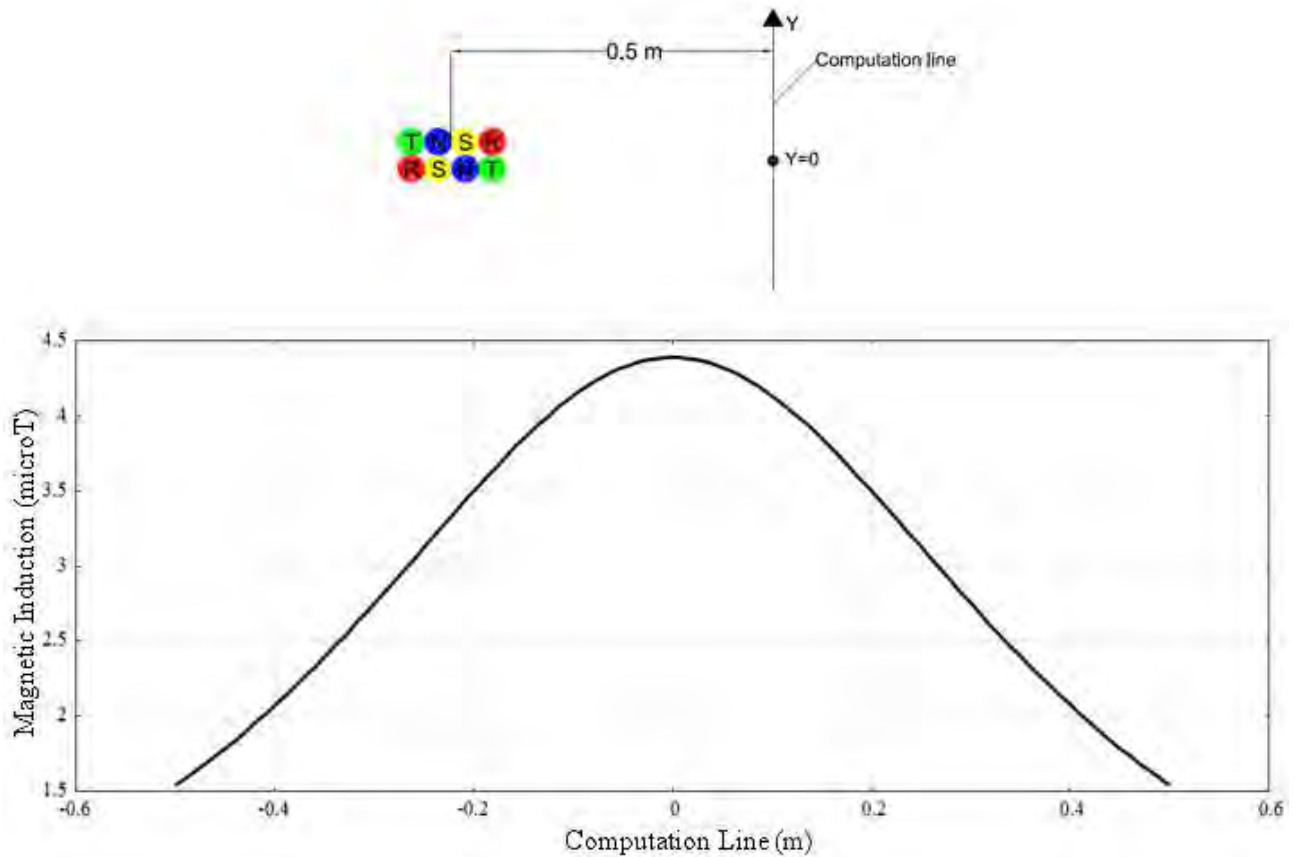

Figure 102 Magnetic induction generate by a LV power lines crossed by a current of 909 A with a mismatch on a single phase equal to 200 A, the configuration of the line is show in upper part of the figure.

From the results presented in Figure 101 and in Figure 102 is clear the influence of the mismatch in relation to the configuration of the line.

The improvements presented above have been implemented inside the substation and the measurements were again performed in all the points of the Figure 100. In this case, however, the value of 3 μT, maximum limit chosen, was not exceeded at no point thus ensuring the achieve of the goal.

4.5 Modular shielding system for MV/LV substations

In this paragraph a complete study of a modular shielding system have been presented. The study is a bit different to the other described in the previous section because in this case is not design a shielding system for a specific application but a modular one suitable for different applications.

The adopted materials are ferromagnetic (isotropic or grain oriented iron), and conductive (aluminum). The combination of ferromagnetic and conductive sheets allows to reach a good compromise between the performance of the two materials both close and far to the shielding system [32]. Several numerical simulations, based on Finite Element Method (FEM), are performed in order to design the best multilayer shield configurations in terms of weight, cost and shielding performance. The first part of this section is dedicated to the simulation of the single slab of pure material, ferromagnetic or conductive. Such activity is mainly devoted to the identification of the physical characteristics as the relative permeability of the ferromagnetic material. The identified material parameters are then used in the simulation of different shielding configurations and, finally, three different multilayer shield compositions are tested and presented.

 The second part of the chapter is devoted to emphasize the key points for assuring a good shielding efficiency in the actual realization of a multilayer shield. The attention is mainly focused on the possible decay of the shielding performance due to the discontinuity among the different slabs. A possible solution of the problem has been identified by means of experimental measurement. The result will be presented and discussed.

In the third section part a substation prototype is developed in order to test the multilayer shield under actual working conditions. An MV/LV substation has been reproduced in laboratory using a 630 kVA transformer working at its rated power and supplied with the system described in section 3.2. Several configurations have been tested and the most interesting results will be presented.

4.5.1   Design of a single part of the shielding system

As shown in the previous application passive shields are usually made of ferromagnetic material with high permeability and conductive material with high electrical conductivity. The combination of ferromagnetic and conductive sheets allows a good compromise between the two types of materials both close and far to the shielding system. Assuming that the screen is interposed between source and the shielded area, the shielding factor of ferromagnetic material is high close to the screen, on the side of the shielded area, but it decreases quickly moving away from the shield. Conversely, the conductive material has a smaller SF close to the screen with respect to the ferromagnetic one. But it keeps a higher SF moving away from the screen. Moreover, the conductive material has better performance on open shield which is the classical case in substation because it can not be locked inside a closed box without an entrance.

Prior to design a shielding system it is required a material characterization based on comparison between experimental results and numerical simulations. A proper setup has been created in order to provide such comparison. As shown in Figure 103 a magnetic source composed by a circular coil properly supplied has been realized in order to create in the centre of the shield a magnetic flux density of 10 and 100 μT (medium and high magnetic induction for ELF magnetic field). The test procedure evaluates the performance of the screen for different distances from the shield. Five inspection points have been defined according to Figure 103.
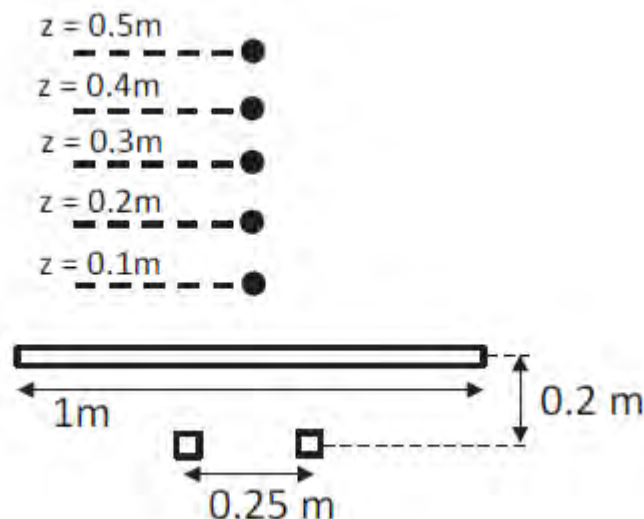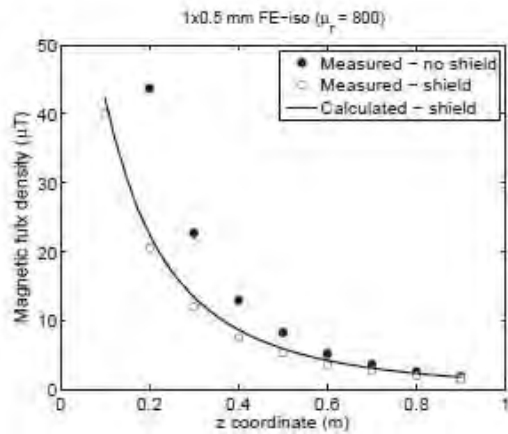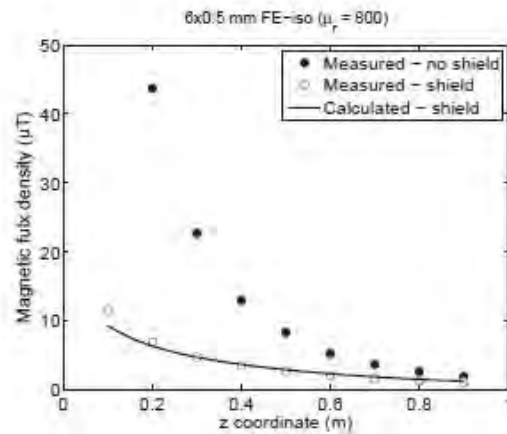

Figure 103 Cross section of the test layout: a circular coil with diameter equal to 0.25 m is placed below the metallic square slab. Five field points are defined in the shielded region The coil is regulated in order to test the shield at two different magnetic field level: 10 μT and 100 μT.

The simulation of this system requires the solution of the Maxwell equations. These kind of problems can be solved by analytical methods only if the geometry is very simple [33] [34]. Conversely, when the geometry is more complicated other approaches must be employed. In this paper the geometry can be easily approximated by a 2D axial-symmetric problem that is handled by the free finite element code that provides magnetic flux density distributions for DC and AC sources [19]. Through the simulation it is possible to verify or identify the actual magnetic and electric characteristics of the shielding materials. In particular in the case of ferromagnetic materials, isotropic or grain-oriented iron (FeGO), the simulation allows to identify the relative magnetic permeability at low magnetic field (from 10 to 100 µT) which is not a technical information provided by the manufacturers of lamination coils; such kind of lamination are usually adopted in electrical machines where the working magnetic flux density is usually higher than 1 T.
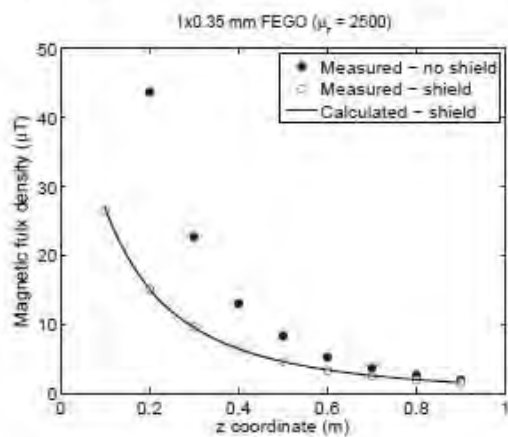
The identification of the relative permeability has been done in the case of one sheet, 0.5 mm of thickness. As shown in Figure 104 (a) a relative magnetic permeability of 800 allows a good matching among experimental and simulation results. The validity of the approach is demonstrated in Figure 104 (b) where the same permeability is adopted in the simulation of a shield composed by 6 sheets. The identification of the FeGO material is a little bit complicated due to the anisotropy of the material. The numerical code allows the identification of an equivalent isotropic permeability that in the case of only one sheet is equal to 2500 (Figure 104 (c)). In the case of couples of layers, alternatively disposed as in Figure 104 (d), the magnetic field find always a low reluctance path. This solution allows to get good shielding performances independently from the location and the geometry of the source. In the case of a couple of FeGO alternate layers the average magnetic permeability become equal to 7500 as shown in Figure 104 (e) (three times higher than one layer). This value is validated in the case of two couple of FeGO alternate layers, as show in Figure 104 (f).
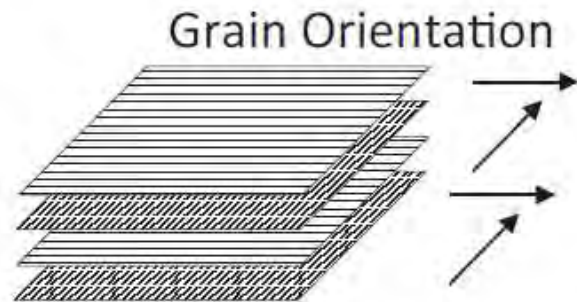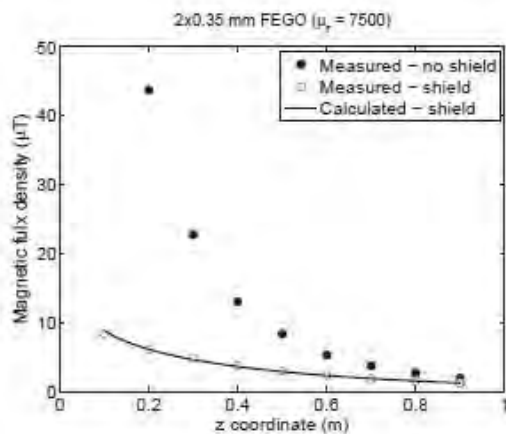
(a) Shield type: 1*0.5mm FE-iso
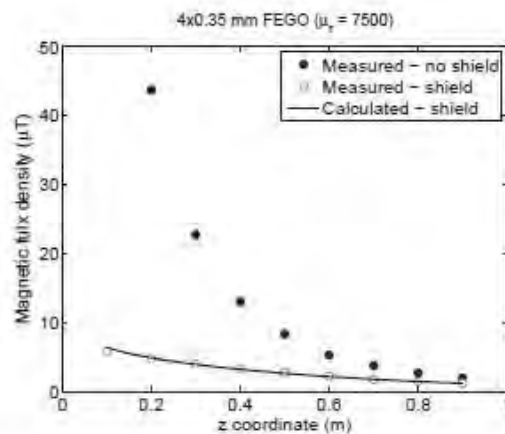
(b) Shield type: 6*0.5mm FE-iso

(c) Shield type: 1*0.35mm FeGO

(d) FeGO disposition in the multilayer shield

(e) Shield type: 2*0.35mm FeGO

(f) Shield type: 4*0.35mm FeGO

Figure 104 Shielding performance of ferromagnetic material: the figure shows measured values for both unshielded and shielded configuration. Moreover, the continuous line represent the result obtained by means of the 2D FEM code.

In the case of pure conductive shielding made of "electrical" aluminum (99.5% of aluminum) the matching between numerical and experimental results is easy to obtain because the electrical conductivity is well known (35 MS/m). In Figure 105 (a) and Figure 105 (b) the comparisons between numerical and experimental results are reported for two different shields having respectively a thickness of 5 mm and 10 mm.

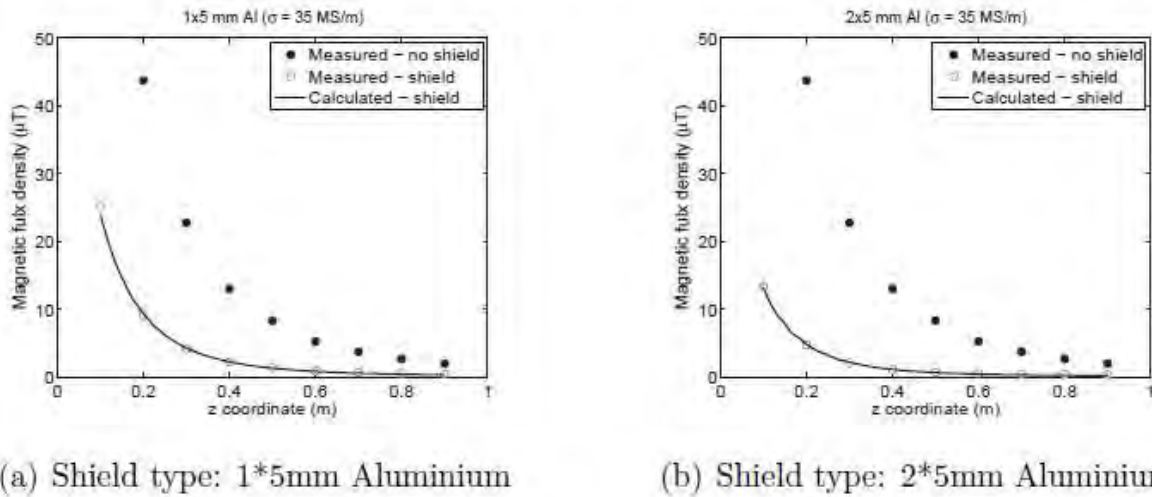(a) Shield type: 1*5mm Aluminium   (b) Shield type: 2*5mm Aluminium

Figure 105 Shielding performance of conductive material: the figure shows measured values for both unshielded and shielded configuration. Moreover, the continuous line represent the result obtained by means of the 2D FEM code.

The use of a mixed shield composed by ferromagnetic and conductive materials provides a further improvement of the magnetic performance. In particular the ferromagnetic material greatly reduces the magnetic field close to the shield while the conductive one tends to maintain a significant shielding factor at higher distance from the shield. In Figure 106 (a) the magnetic flux density versus shield distance is reported for the case of a multilayer shield composed by a sheet of aluminum (5 mm of thickness) and 2 layers of FeGO (each one is 0.35 mm of thickness).

(a) Al 5mm FeGO 2*0.35mm (FeGO on the side of the source)

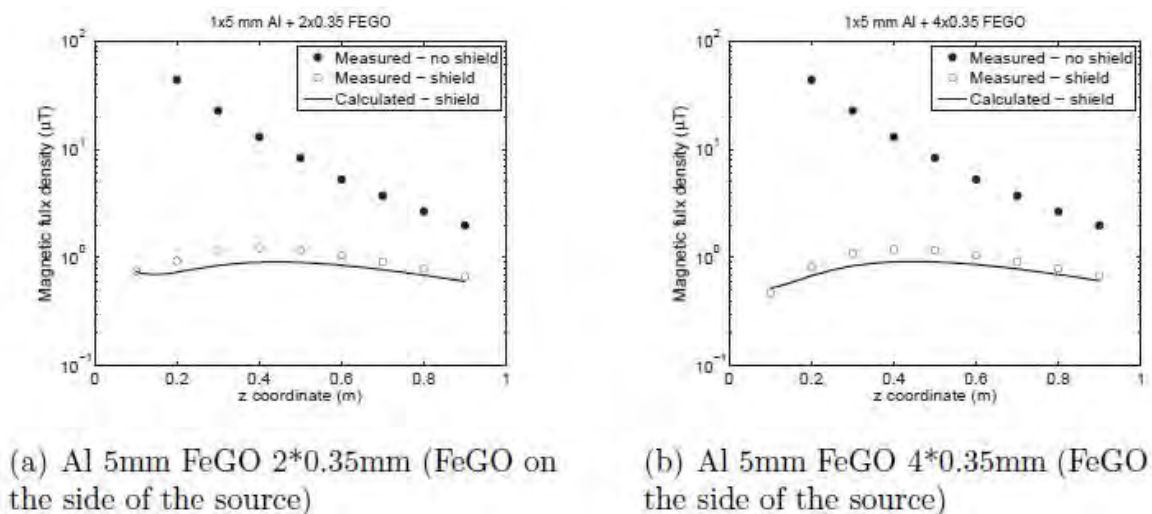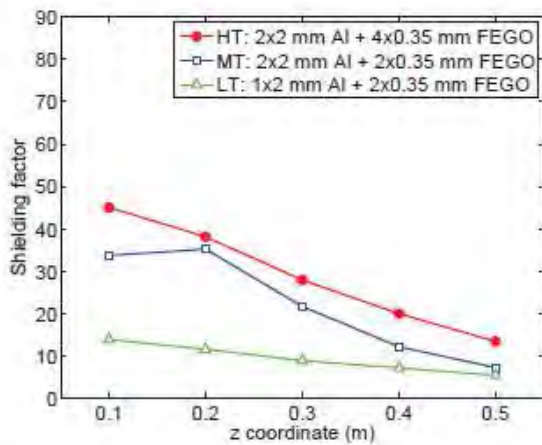(b) Al 5mm FeGO 4*0.35mm (FeGO on the side of the source)

Figure 106 Shielding performance multilayer slabs: the figure shows measured values for both unshielded and shielded configuration. Moreover, the continuous line represent the result obtained by means of the 2D FEM code.

In Figure 106 (b) the shield is composed by a sheet of aluminum (5 mm of thickness) and 4 layers of FeGO (each one is 0.35 mm of thickness).
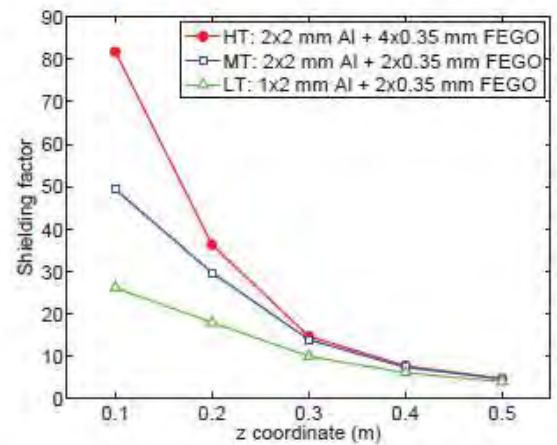
The two charts are reported in logarithmic scale in order to better point out the good performance of the two shields and the good matching between calculated and measured values. The validation of the simulation procedure makes possible to virtually design the shield avoiding other experimental tests. En extensive and detailed simulation activity has been carried out considering material combinations, number of slabs, thickness, disposition, etc. A set of three different configurations have been found in order to fulfill the most common mitigation requirements in substations. The three multilayer shields are constituted by the following composition:

• "LT" Low Thickness Shield: Al 2mm FeGO 2x0.35 mm

• "MT" Medium Thickness Shield: Al 4mm FeGO 2x0.35 mm

• "HT" High Thickness Shield: Al 4mm FeGO 4x0.35 mm

In Figure 107 the shielding factors associated to the three shields are reported for the case of Al or FeGO faced to the source, respectively. It is possible to verify that when the Al is faced to the source a lower shielding factor close to the shield is measured, but the shielding performance are maintained far from the shield.

(a) Shielding factor with Al on the side of the source

(b) Shielding factor with FeGO on the side of the source

Figure 107 SF of the three multilayer slab configurations: HT (cirle-red), MT (empty circle-blue), LT (empty triangle-green)

4.5.2 Influence of the connection among slabs

Generally, in order to mitigate a substation, more than one slabs will be necessary. therefore, a critical point is the assembly of elementary plates because it is characterized by an unavoidable magnetic and electric discontinuity. For open shields the discontinuity of the ferromagnetic properties is less important, therefore, particular attention has been dedicated to the conductive parts. In Figure 108 (a) a schematic representation of the induced currents in the case of a homogeneous conductive plate is shown. Figure 108 (b)
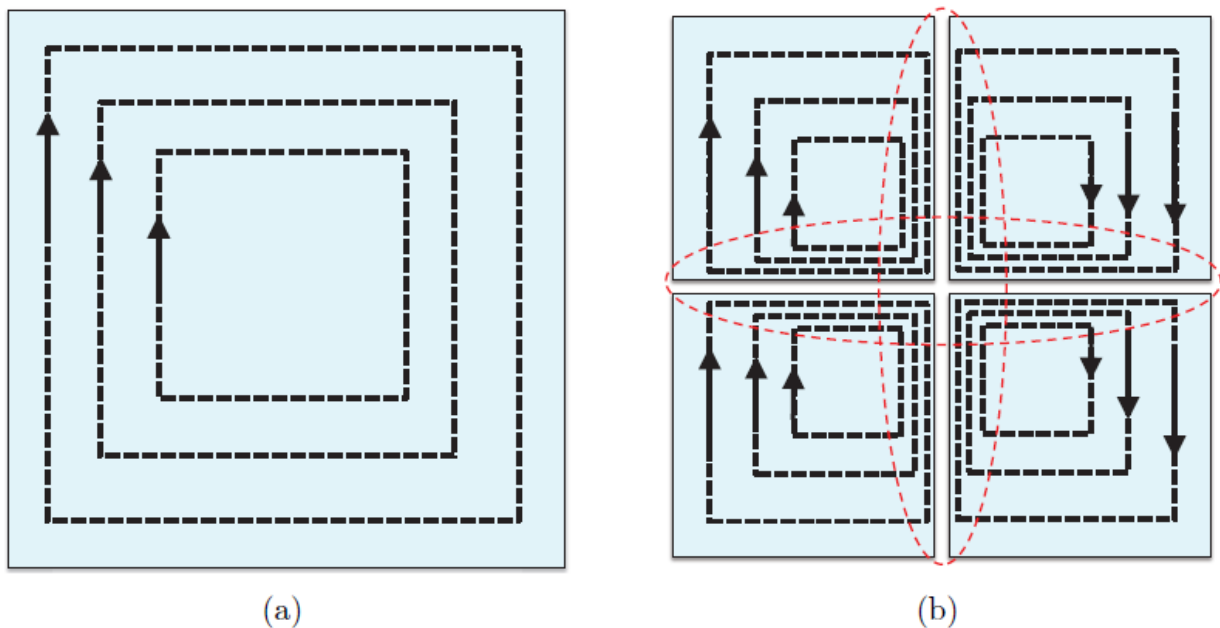

(a)

(b)

Figure 108: Effect of the discontinuity among slabs: figure (a) represents the induced current paths for a single and continues metallic slab with the same size of four smaller slabs. In figure (b) the four separate slabs are represented with their own induced current path.

The simulation of not connected shields should require a 3D numerical approach however, in the practical applications the metallic slabs will be joined each other by means of a some straight bars made of aluminum. A single bar is superposed and fixed to two adjacent slabs by means of some rivets. Nowadays it is still quite difficult to simulate with good accuracy this kind of connection because it is characterized by two surfaces that are not in perfect contact. Therefore, in the present paper the problem has been directly investigated by an experimental approach through the setup presented in Figure 109. Four square HT plates with side length equal to 1 m are considered and in Figure 109 (a) it is possible to observe the field source. It is a square coil having the same edge of the single plate. It is placed below the shield at 0.5 m of distance. The shield performance are

evaluated on the nine inspection points defined in Figure 109 (b). They are located in a plane that is 0.5 m above the four slabs.
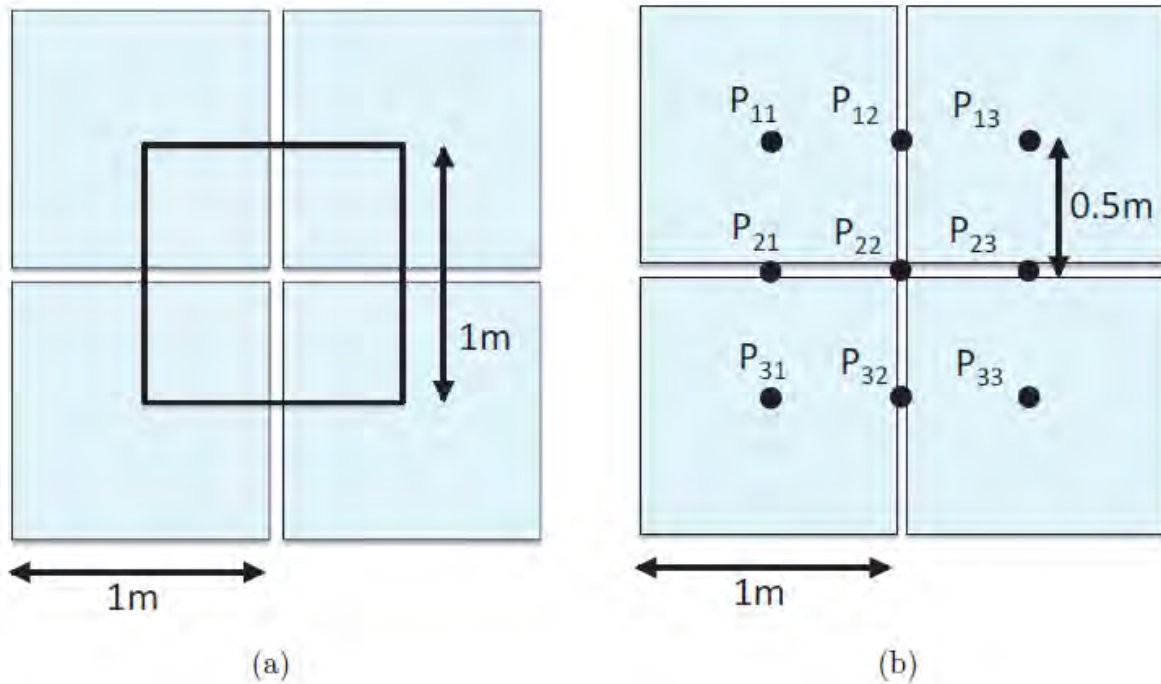

Figure 109 Setup for the evaluation of the performance decay for not connected shield. A square coil (side of 1 m) is centered with respect to the four slabs and placed 0.5 m below them (a). Nine inspection points are defined in a plane located 0.5 m above the four slabs (b).

Four different cases are analyzed:

• Case 1: separate slabs and Al faced to the source
• Case 2: separate slabs and FeGO faced to the source
• Case 3: connected slabs and Al faced to the source
• Case 4: connected slabs and FeGO faced to the source

In Table 6 the measured SF are summarized. It is highlighted the row corresponding to the central inspection point (P_{22}) and the column of the solution with the higher SFs. It is apparent that restoring the conduction among plates the overall performance of the shield is improved. Moreover, it is interesting to note that in case of separate slabs the configuration with FeGO faced to the source allows to reach higher SFs for almost all inspection points. However, this values can be roughly

doubled if the connection among the slabs is restored. In this case, as expected, the shielding factor is higher when the aluminum is faced to the source.

Field Point	Case 1 SF	Case 2 SF	Case 3 SF	Case 4 SF
P_{11}	1.98	2.50	4.53	3.34
P_{12}	2.45	2.71	5.39	4.03
P_{13}	2.06	2.61	4.47	3.57
P_{21}	2.50	2.72	5.49	4.42
P_{22}	3.22	3.18	6.72	5.71
P_{23}	2.56	2.82	5.45	4.68
P_{31}	2.15	2.64	4.52	3.59
P_{32}	2.63	2.71	5.23	4.51
P_{33}	2.55	3.07	5.14	4.53

Table 6 SF for connected and not connected shield

4.5.3 Experimental test on a substation prototype

The shielding efficiency related to the final mitigation system must take into account the actual geometry of the source and shield. In this paper the global performance is tested on a substation prototype. It is composed by a 630 kVA cast resin transformer and its LV conductors. An aluminum structure has been created around the transformer in order to test any possible shield configuration.

In this subsection the performances of different shielding configurations are presented. Of course the extension of the shield is linked to the use of the neighbouring areas. In addition to that the shielding performance depends on the geometry and the extension of the shield. For all the configurations the HT solution has been used and the magnetic flux density have been measured by a proper magnetic field probe. The basement of the shielding structure is placed at z=0. Two different planes has been analysed: at 1m and 4.4.m. The quote of 1 m is important because it is the average height of the sensitive parts of the human body and correspond, around the substation, to the quote of the low voltage terminals of the transformer where the magnetic pollution is significant. The other quote is representative of what happening in the area above the transformer. In Figure 110 and in Figure 111 are reported the field point distribution respectively at the levels of 1 m and 4.4 m.
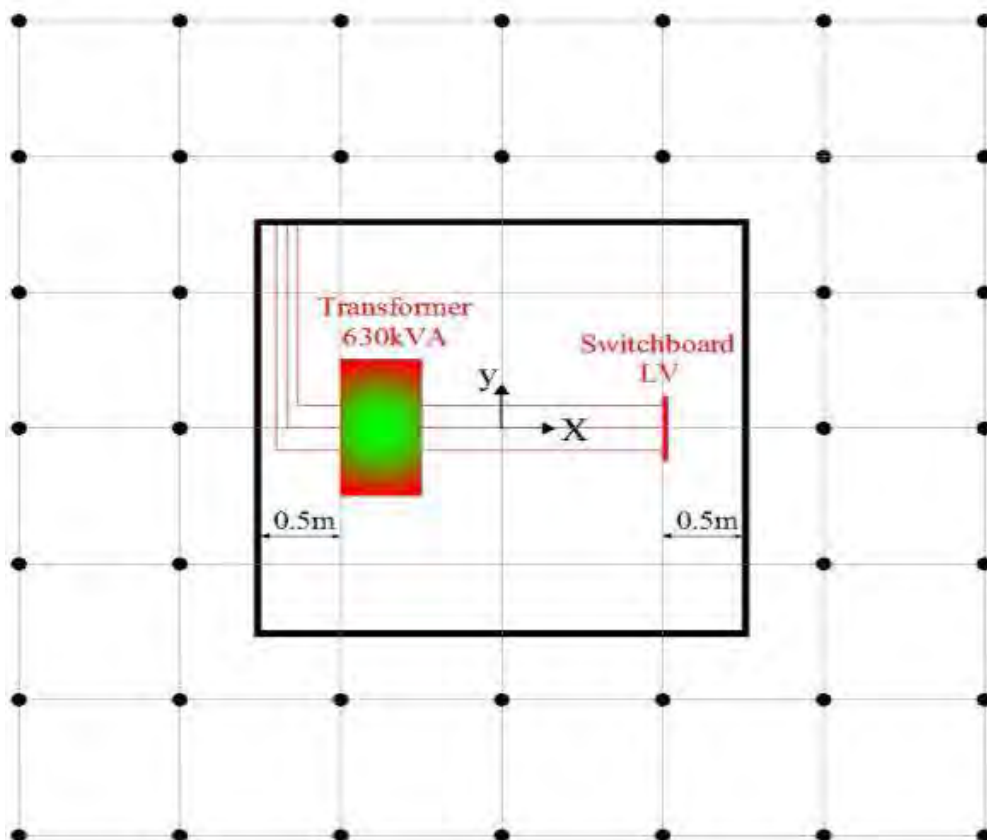

Figure 110 Field measurements points at z=1m

The measurement of magnetic flux density relatively at the two planes are shown respectively in Figure 112 and Figure 113 where it possible to see how the limit of 3 µT is overcame in all the planes.
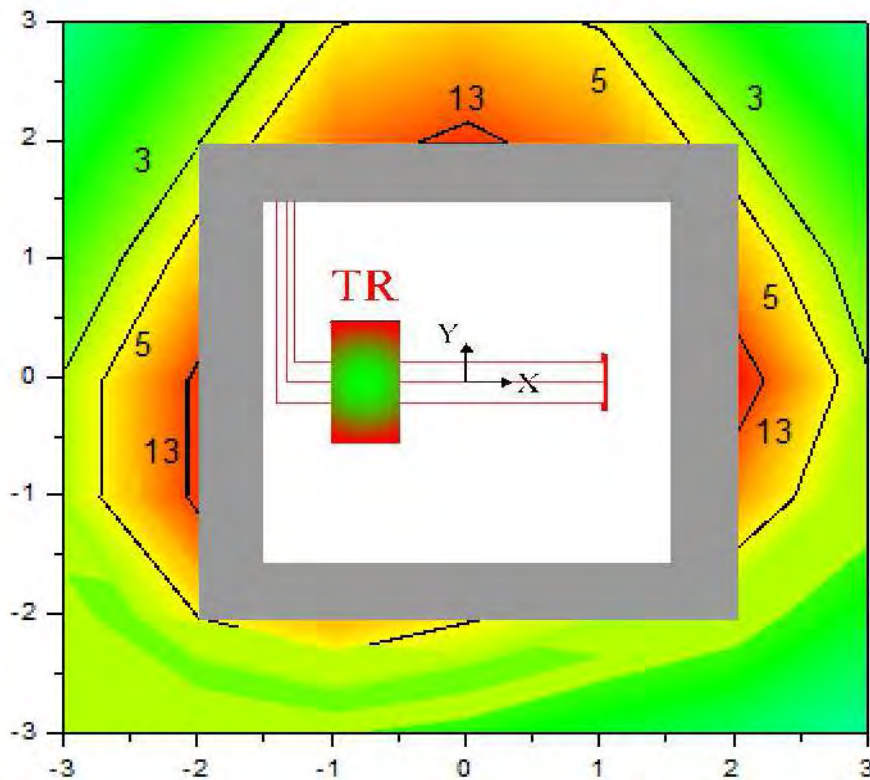

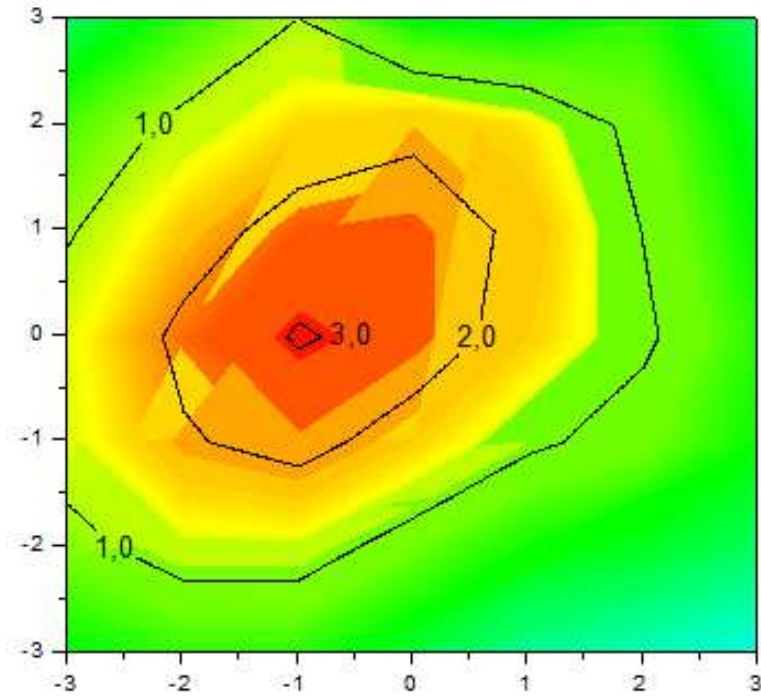Figure 112 Magnetic flux density coloured map at z=1m due to source (without the shield)

Figure 113 Magnetic flux density coloured map at z= 4.4 m due to source (without the shield)

In a first analysis two shield configurations, reported in Figure 114 and Figure 115 , are build in order to reduce the magnetic pollution above the substation (Conf_1 and Conf_2). The two configurations are different in terms of extensions (9 sqm and 21 sqm), and in terms of end effects contribution.

Figure 114 Shielding only on the substation ceiling (Conf. 1)

Figure 115 Shielding on the substation ceiling and on the side for 1m high (Conf. 2)

End effects can happen both in ferromagnetic and conductive materials and can produce a local increase of the magnetic fields. Of course, in such comparison the shield Conf_1 produces in the area above the substation an higher end effect compared to the shield Conf_2. In the shield Conf_2 the end effects are strongly reduced due to the lateral appendages (1m high). The improvement of shielding performances of the Conf_2 compared to the Conf_1 is evident in Figure 116 and Figure 117: the Conf_2 allows to reach approximately twice shielding factor.
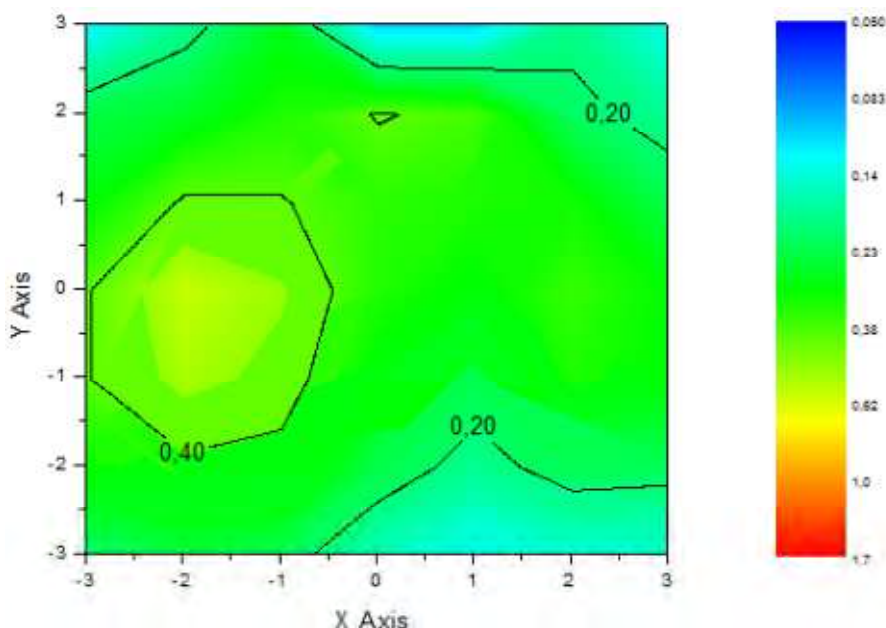

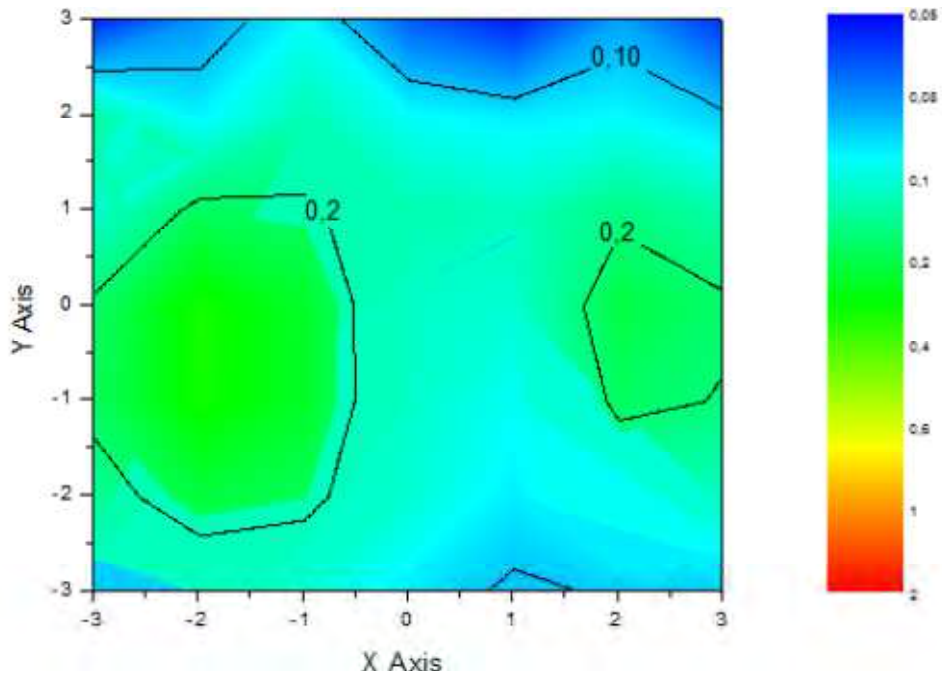Figure 116 Magnetic flux density coloured map at z= 4.4 m with the shield of Conf. 1

In order to shield also the areas at the same level of the substation, additional shield elements are installed on the lateral sides starting from the Conf_2. Two configurations are considered: in the first configuration (Figure 118– Conf_3) the shield is placed in the two lateral sides parallel to the transformer, in the second one (Figure 119– Conf_4) all the sides are shielded.

128

Figure 119 Shielding on all the sides of the substation (Conf. 4)

With the shield on the substation sides, the magnetic field in strongly reduced also at the quote of 1m. In Figure 120 can be observed how the Conf_3 do not allow a complete reduction of the magnetic field under the level of 3 µT, anyway ad average value of 1 µT can be found around the substation
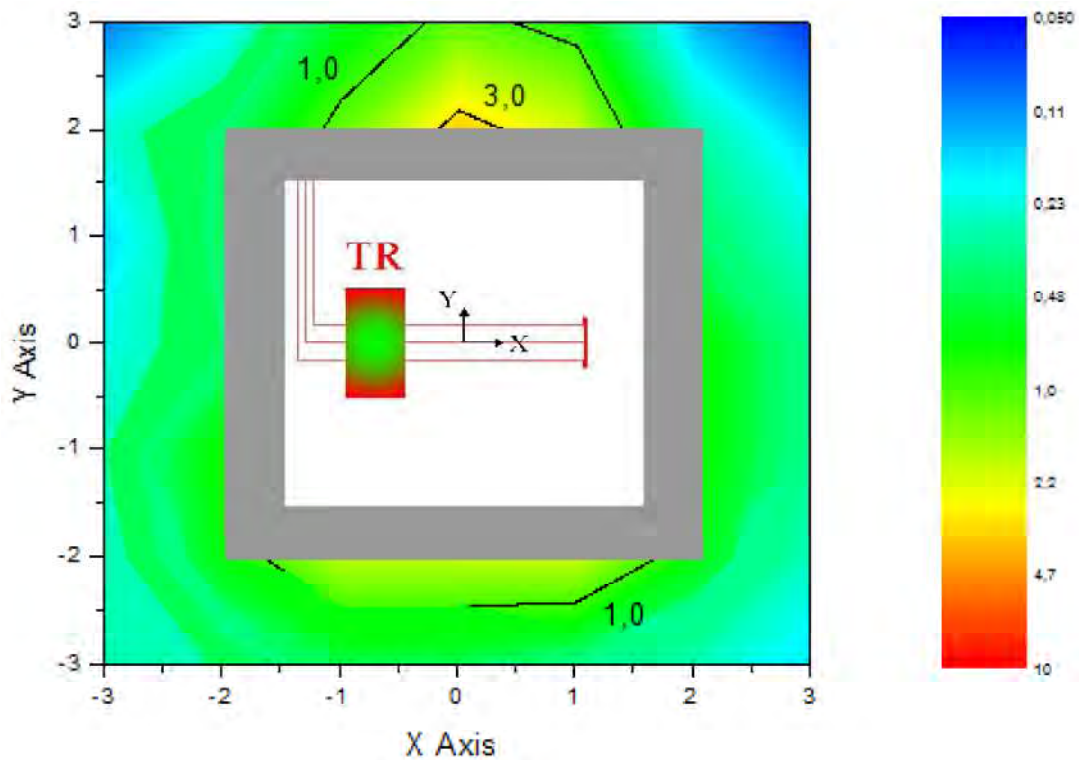

Figure 120 Magnetic flux density colored map at z= 1 m with the shield of Conf. 3

In Figure 121 is shown how the Conf_4 allows a significant reduction in all the sides except in front of the door side of the substation.
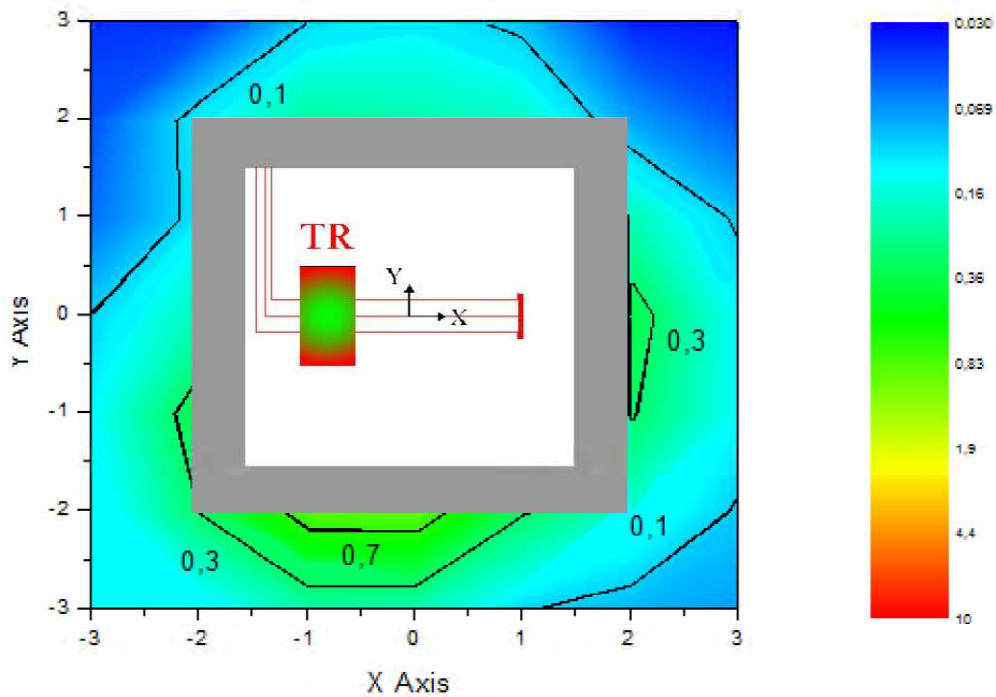

Figure 121 Magnetic flux density coloured map at z= 1 m with the shield of Conf. 4

Figure 122 and Figure 123 shows that the magnetic reduction above the substation is almost the same for the two configurations. This means that the lateral appendages of 1 m (Conf_2) are sufficient in order to achieve the shielding of magnetic field above the substation.
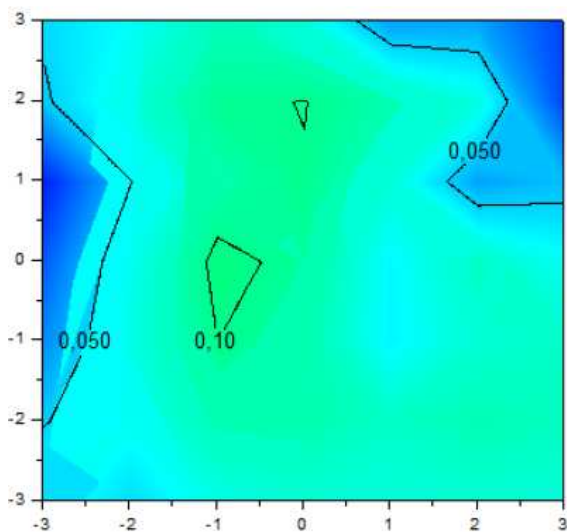

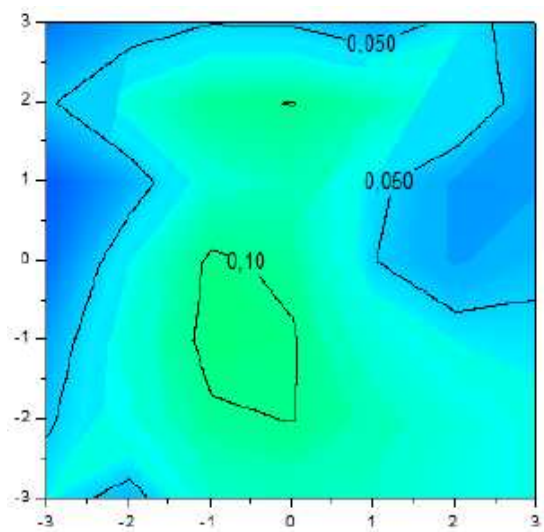Figure 122 Magnetic flux density coloured map at z= 4.4 m with the shield of Conf. 3

Figure 123 Magnetic flux density coloured map at z= 4.4 m with the shield of Conf. 4

Finally in Figure 124 and in Figure 125 the shielding factors evaluated in the plane at 1 m and 4.4 m are reported. As can be observed, the SF is higher than 30 close to the source, and it is approximately higher than 15 at 1m from the shield. Such higher values allow to achieve the required performances in all the areas close to the substation.
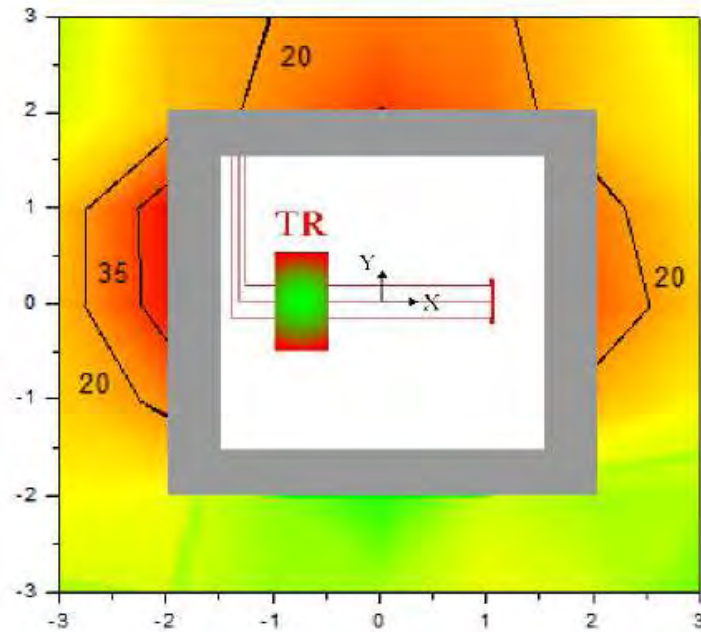

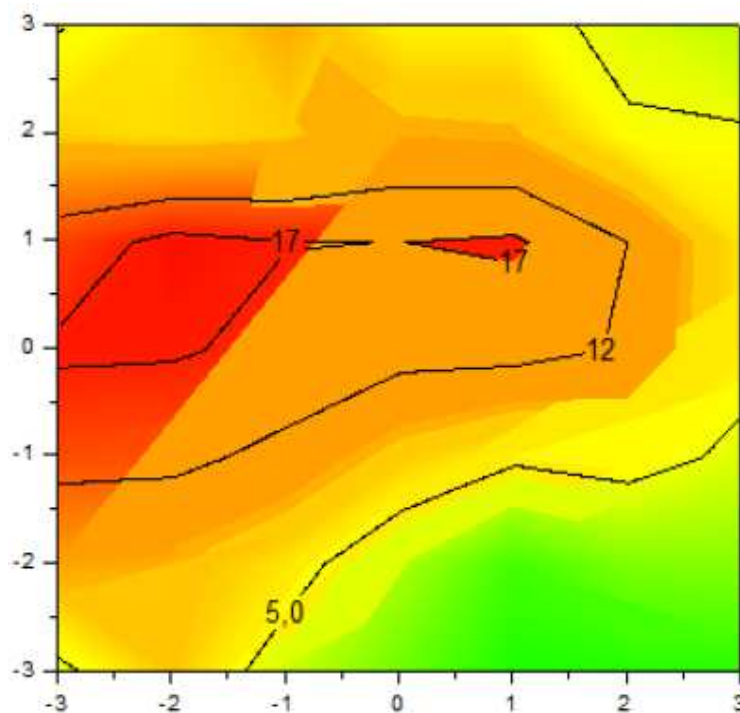Figure 124 Shielding factor colored map at z= 1 m with the shield of Conf. 4

Figure 125 Shielding factor density colored map at z= 4.4 m with the shield of Conf. 4

4.5.4   Conclusion

The paragraph deals with the design of multilayer magnetic shields made of ferromagnetic (FeGO) and conductive material (aluminum). A detailed simulation activity has been performed in order to identify the magnetic and the electric characteristics of the employed material.

The problem of the unavoidable discontinuity of the slabs when significant shielding surface has to be realized have been analyzed. The solution is based on the restore of the electrical connection of the conductive parts of the slabs using some straight bars made of aluminum to connect the slabs to each other.

At the end different geometrical configurations, composed by the slabs studied, have been analyzed in order to evaluate the effect of the shielding size. The reduction of the magnetic field is strongly influenced by the shield extension and a significant improvement in shielding performances is obtained when the shield is not limited to the surface between the source and the "victim" but has additional element on the lateral sides. The shielding factor can rise value also value of 35 and globally, around the substation, the shielding factor values are enough for satisfying the objective of a magnetic induction of 3 μT.

4.6   Shielding system for a complex substation

The last described application deal to the analysis of magnetic field generated by a complex MV-LV substation and the application of 3 suitable shielding techniques are presented. The substation consists of 19 transformers with rated power ranging from 1600 up to 2500 kVA, and it is built near a datacenter which allows a maximum magnetic flux density value of 1 μT. Firstly, a base case of an usual installation of the substation is analyzed, in order to calculate the magnetic flux density generated. At this regard, an integral 3D model of the magnetic field has been arranged for each device in the substation: MV/LV transformer, MV and LV switchgears, power lines. Therefore, 3 shielding techniques are proposed and implemented: the transposition of transformers, the transposition of conductors, the installation of multi-layer shielding plates on walls. First two methods consists on the optimization of the arrangement of transformers and conductors in the substation according to installation requirements, the last method is based on the conductive and ferromagnetic shielding effect of multi-layer plates installed on the walls of the substation, in order to achieve a mitigation in the external environment. Finally, some measures of magnetic flux density on the real substation which implements the 3 techniques are performed, in order to estimate the shielding factor with respect to the base case.

4.6.1 Base configuration of the MV-LV substation

The case study is a complex substation consisting of 19 cast resin transformers with rated power ranging from 1600 up to 2500 kVA.

Figure 126 shows the base configuration of the MV-LV substation, in which transformers and power lines are configured as in a usual substation.
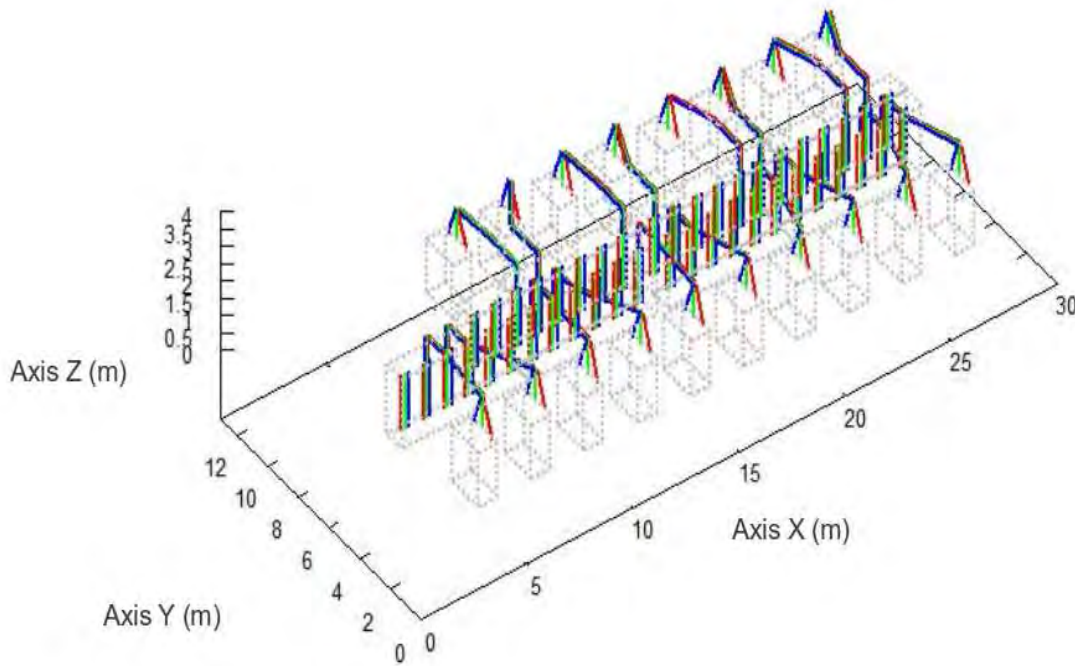

Figure 126 Base configuration of the MV-LV substation

Figure 127 reports the results of a calculation of magnetic flux density on a XZ inspection plane, with Y = -1 m regarding the base configuration. The calculation is performed with the integral models described previously. The maximum value of B is 35 µT RMS.
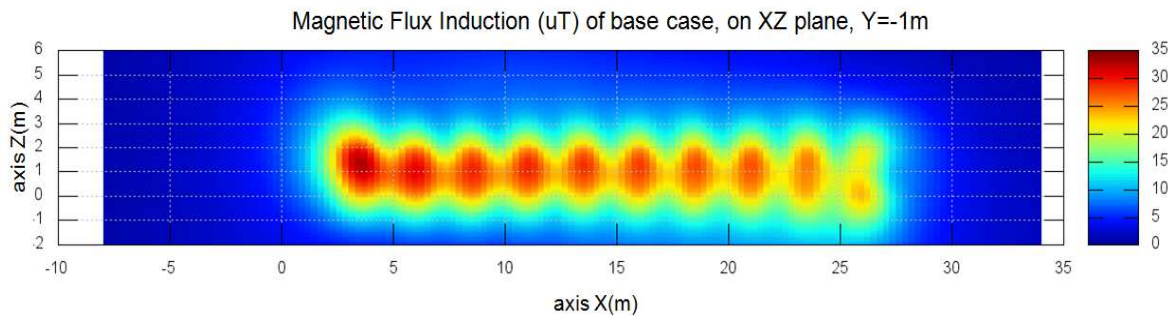

Figure 127 Magnetic Flux Density calculation in µT on a XZ inspection plane, with Y = -1 m

4.6.2   Transposition of the transformers

The technique of mitigation of magnetic flux density applied in this second configuration of the MV-LV substation is the transposition of the transformers. The cables of two consecutive transformers are arranged in an opposite way: L1 L2 L3 on one transformer, L3 L2 L1 on the other one, as represented in Figure 128.
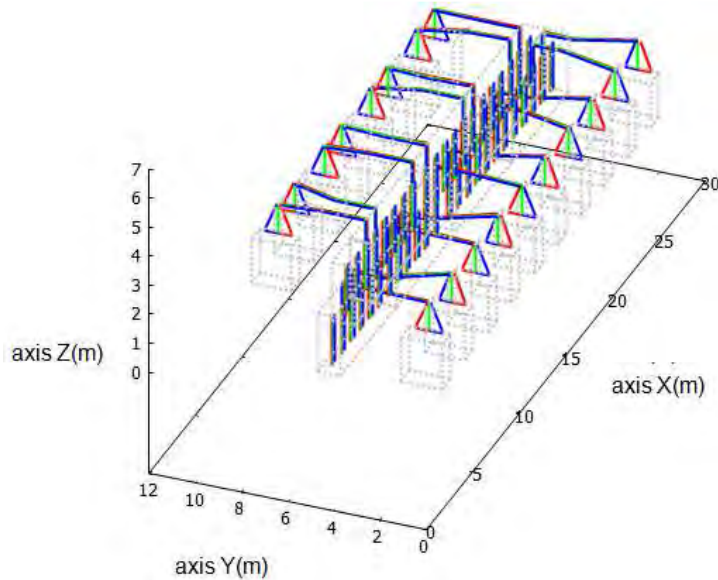

Figure 128 Configuration n.2 of the MV-LV substation: transposition of the transformers

In this way, the level of magnetic flux density on the same inspection plane analyzed before is lower as show by the comparison of Figure 129.
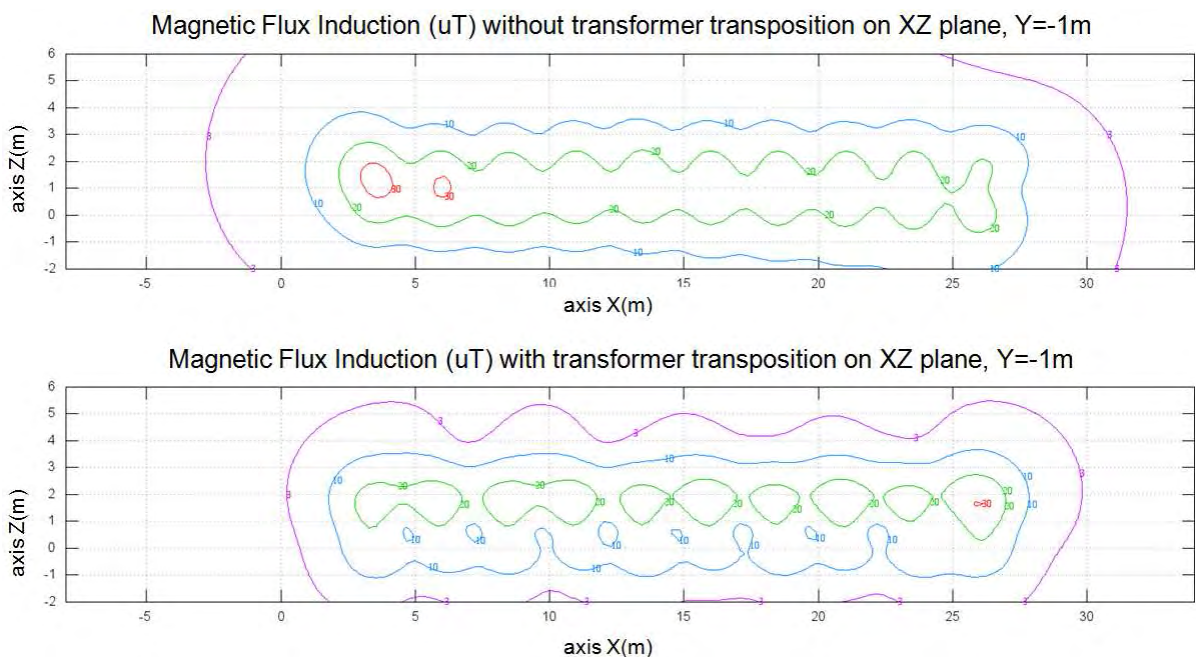

Figure 129 Magnetic Flux Density on a XZ inspection plane, with Y = -1 m in the case of transposition of transformers

4.6.3   Transposition of cables

In this section another technique of mitigation of magnetic flux density suitable for MV-LV substation is presented: the transposition of conductors. The analyzed substation is characterized by 19 power lines which connect the transformers to the LV switchgears. Each power line has 21 conductors: 6 conductors each phase, and 3 neutral conductors. Figure 130 reports the base configuration and 2 optimized configurations for the 21 cables in the duct. As shown in Figure 131 Opt2 is the best solution that minimizes the emitted magnetic flux density, Opt1 is not the best solution, but it is a good compromise between ease of installation and magnetic field emission.
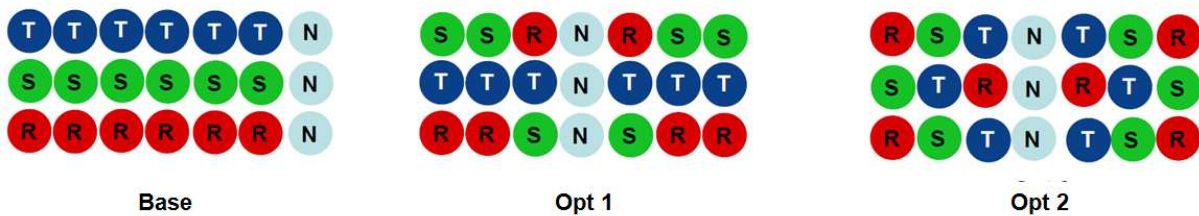

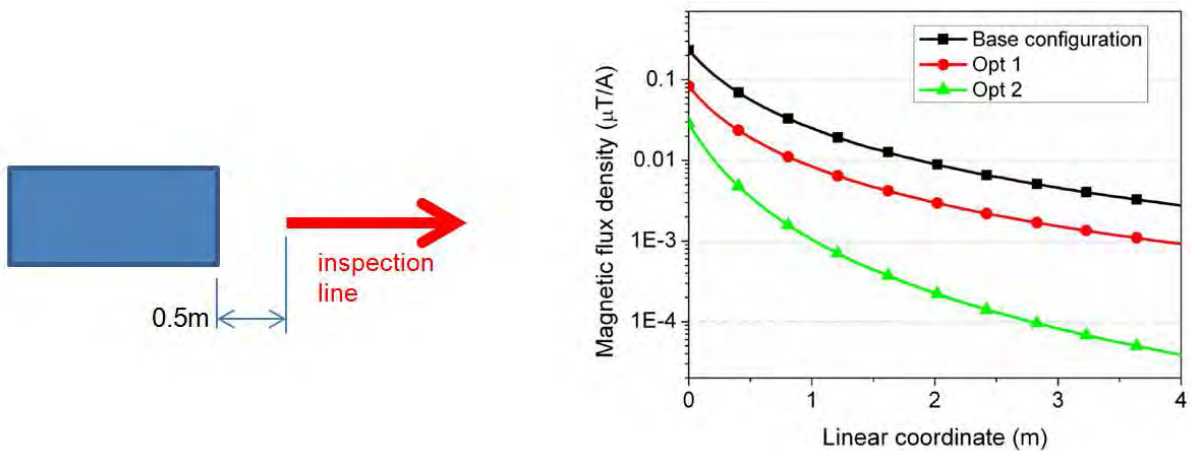Figure 130 Base and optimized configurations of power lines

Figure 131 Magnetic Flux density on the inspection line related to 3 different configurations of conductors in the duct

4.6.4   Multilayer magnetic shielding plates

In this section the shielding technique by flat shielding materials is presented. The adopted flat shielding system is based on multilayer plates, each one composed by a sheet of aluminum (4mm thick) and 4 layers of FEGO (isotropic of grain-oriented iron, each 0.35mm thick)   (shielding system presented in section). Joined conductive sheets are welded in order to allow eddy currents to carry the whole shielding surface

The shielding system has been really installed on the internal surfaces of the substation: the whole floor and the wall on Y=0m (attached to the inspection plane analyzed before) has been covered by the shielding plats. The Figure 132 shows the solution of installation.
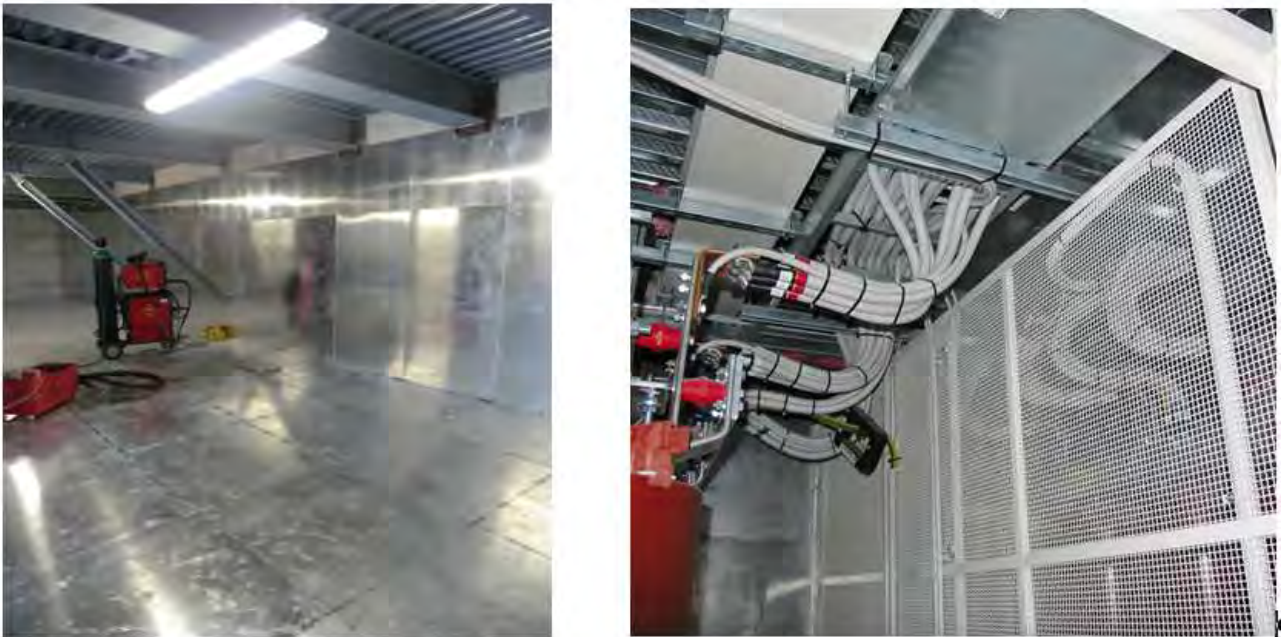

Figure 132 Installation details of the flat multilayer shielding system and implementation of transposition of cables and transformers in the MV-LV substation

4.6.5   Results of the adopted shielding techniques and conclusion

In this section the result of the measures of magnetic flux density, arranged after the implementation of the described shielding techniques, are presented. The adopted shielding techniques are the transposition of transformers, the transposition of conductors, and the installation of the flat multilayer shielding system. A measure of magnetic flux density on an inspection line has been performed, and the result have been compared with the computation performed on the base configuration (without any implemented technique of shielding). The measures have been performed while the current carrying the transformers was 1/6 of the nominal rated current, and also the computation was performed with this value of current. The results are reported in Figure 133, which shows that the average shielding factor on the considered inspection line is 48,5.
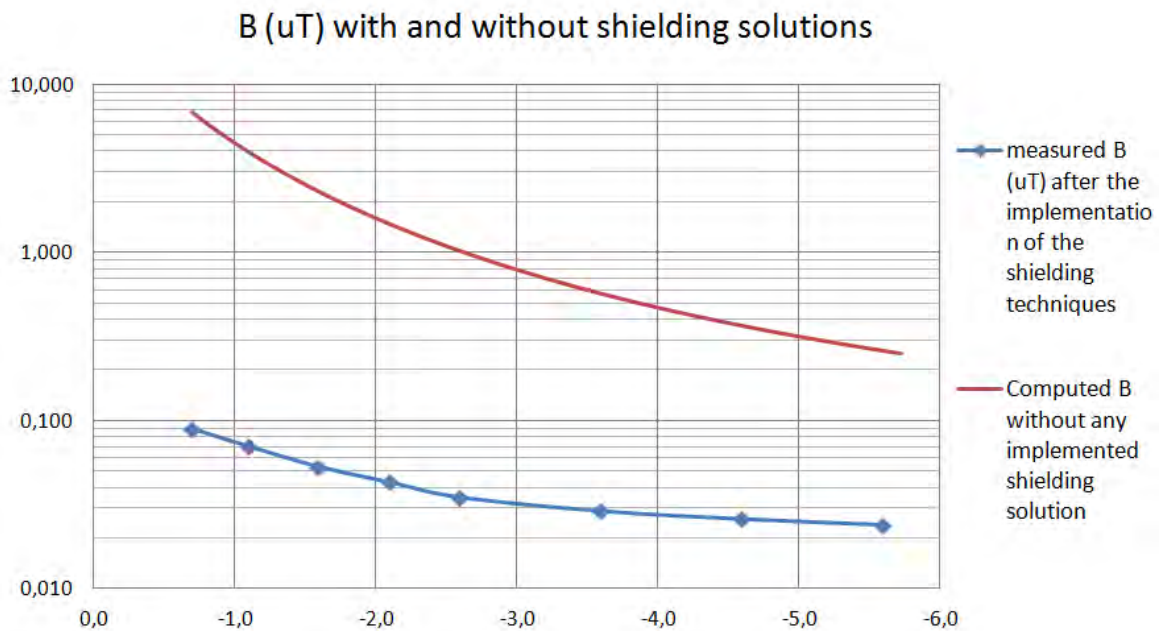

Figure 133 Comparison between measured B after the implementation of the shielding techniques, and computed B of the base case without any shielding solution.

The achieved shielding factor at a distance 1÷5 m from the substation is relative high and the proposed goal (maximum level of magnetic flux density outside the substation) has been reached.

5   Conclusion

The dissertation deals with the modeling and design of magnetic shields for electrical installations.

In the first part the model of the sources of magnetic induction and of the shielding system are presented.

The sources are modelized   linking each component to only three types of sources of electromagnetic induction.

Three models for the analysis of screening system are presented in order to analyze conductive, ferromagnetic and multilayer shield.

In the second part the supply system for the laboratory test are presented, in particular are described the system for the test of the MV/LV transformers and the system for the test of power lines and MV, LV switchgears.

In the third part the analysis of different screening system are shown.

The different cases analyzed were chosen in order to describe different applications as possible so as to show how the possible cases are multiple and can be solved in different ways.

Clearly all the analyzed cases could be treated using different shielding solutions but to be lighter on the elaborate only the final solutions were presented.

The full analysis of the various screening systems therefore include a preliminary phase in which is chosen type of shielding to be adopted for the specific case study.

A preliminary phase of the study of a screening system is presented below. The analysis deal on the design of a shielding system of a building placed under an high voltage power lines [24].

Figure 134 represents a structure below and over head power lines. In Figure 135 the structure is better described. Particularly, the shield is applied to all the walls but the floor. In the figure the suface mesh of the shield is shown. The metallic enclosure is designed with some holes in correspondence of 4 windows and 1 door. The performance of the shield is evaluated on an inspection plane at 2 m from the ground level. Moreover 3 inspection lines are defined. All the inspection lines lay on the inspection plane and, particularly, line 1 is its perimeter.
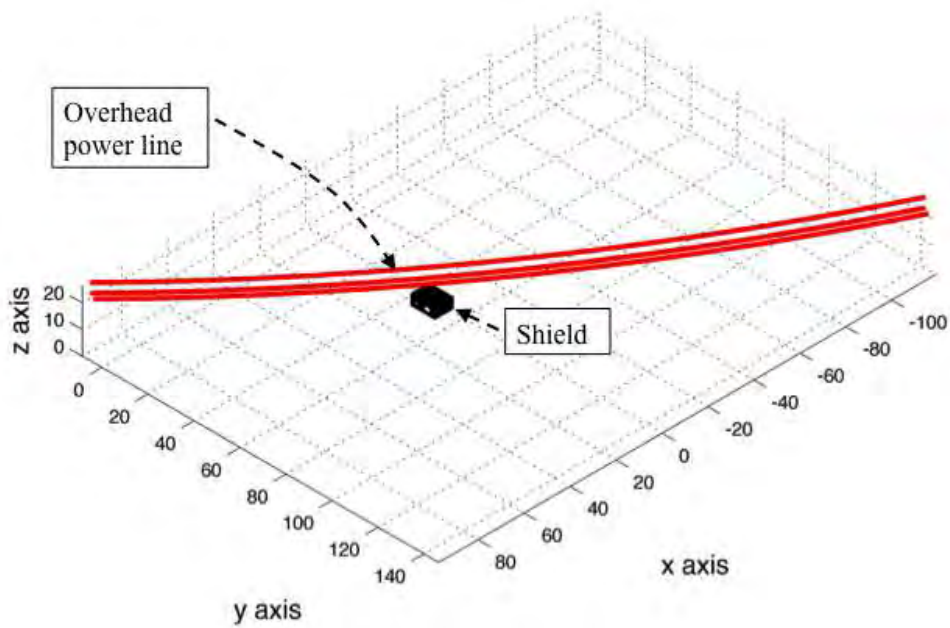
Figure 134 Overhead power line and shielding system The last one encloses all the volume to be shielded

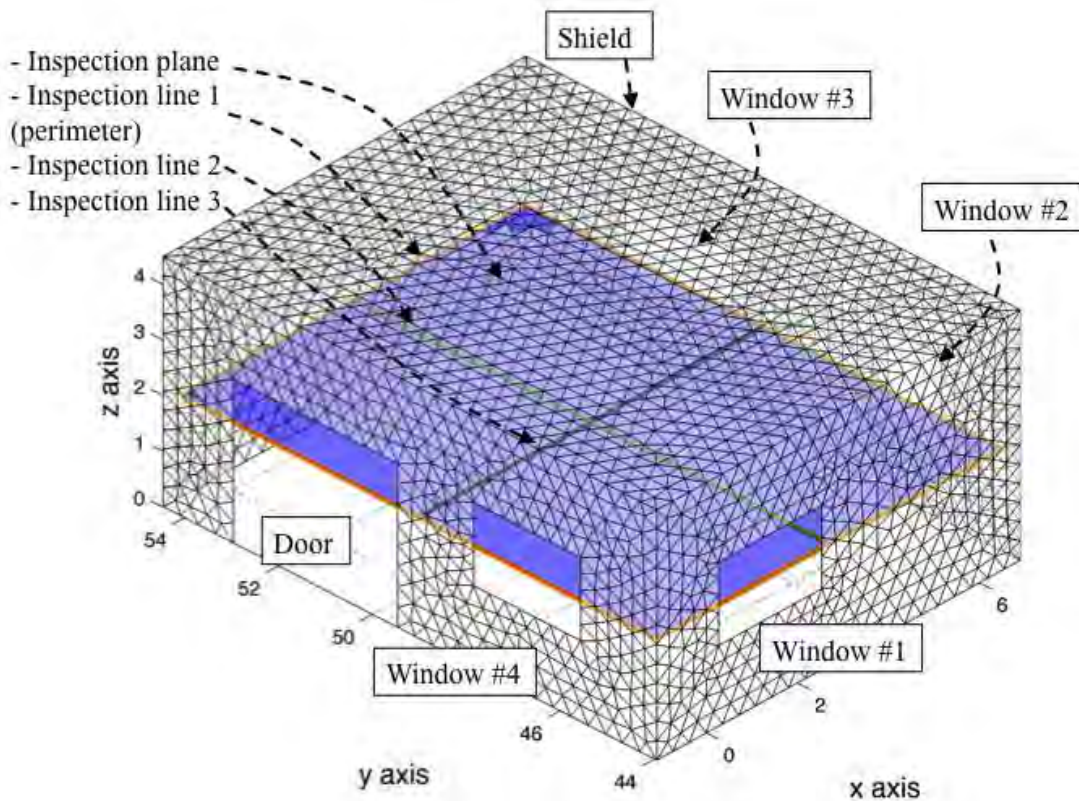**Figure 135 - The shield encloses all the volume where the mitigation is required. The metallic enclosure is designed with some holes in correspondence of 4 windows and 1 door. Different material are considered. Their performance are evaluated on an inspection plane at 2 m from the ground level. Moreover 3 inspection lines are defined. Particularly, line 1 is the perimeter of the inspection plane.**

Two different material are tested: Aluminum with 2 mm of thickness, Grain Oriented Iron (FeGO) with 0.75 mm of thickness.

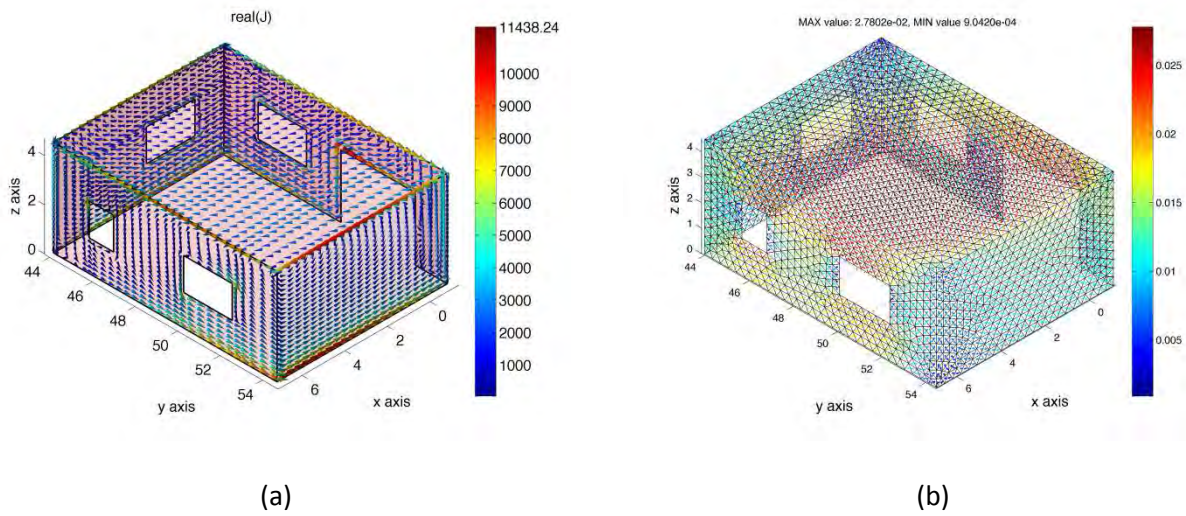(a)   (b)

Figure 136 – (a) Example of eddy current computation (b) example of magnetization computation

Figure 136 represent the main output of the two formulations. In Figure 136 (a) the eddy currents inside the aluminum shield are shown whereas in Figure 136 (b) the magnetization of the FeGO is reported. First of all the source field is computed as shown in Figure 137. It is possible to see that the power line creates higher values in the upper right corner of the inspection plane whereas the lowest value is registered in the opposite corner.
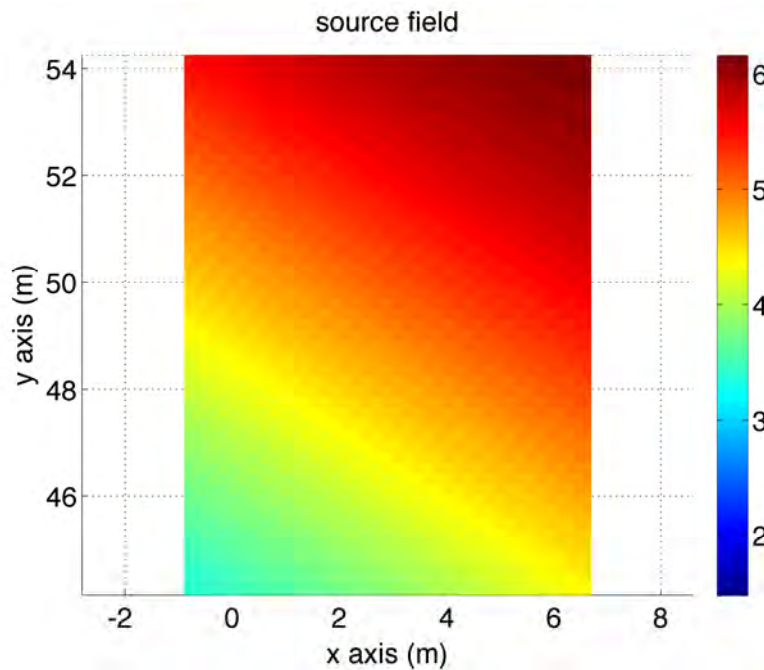

Figure 137 Source field on the inspection plane. Higher values are identified in the upper right corner.

The effect of the shield is shown in Figure 138 and Figure 139 for aluminum ad FeGO, respectively. It is apparent that the mitigation by means of aluminum is stronger.
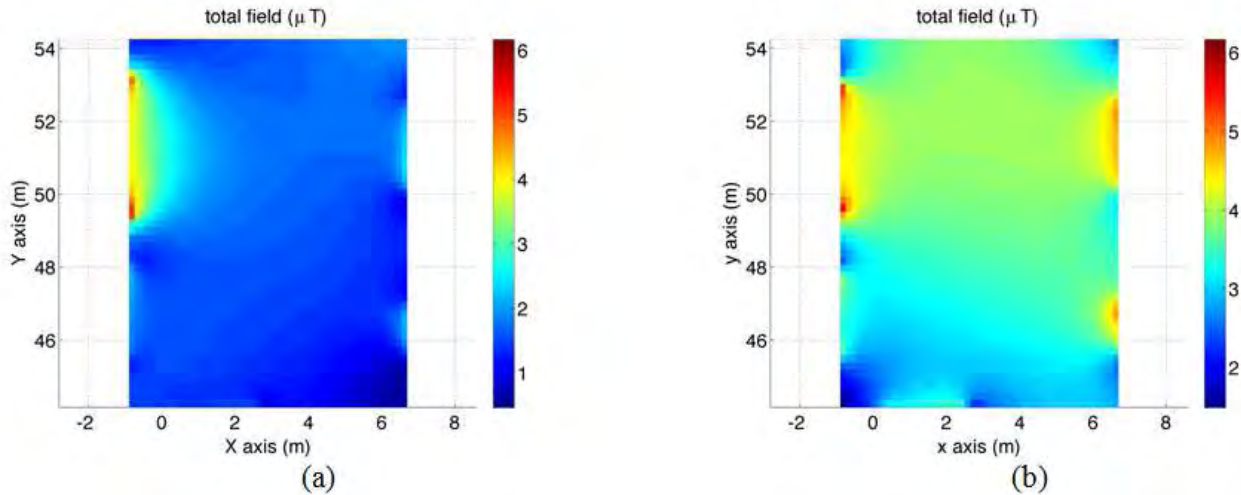

Figure 138 (a) Total field with Aluminum (thickness: 2mm). (b) total field with of FeGO (thickness: 2x0.35).

Figure 139 (a) Shielding factor with Aluminum (thickness: 2mm). (b) shielding factor with of FeGO (thickness: 2x0.35).

To have a more direct comparison the field is also computed along three inspection lines. The inspection line 1 is the perimeter of the inspection plane and the relative magnetic field levels are shown in Figure 140. It is possible to observe that the Aluminum reduces the field below 3 μT in almost all points. Just in front of the door the edge effect are comparable to those of the FeGO shield. Finally, the comparison on the other inspection lines can be observed in Figure 141 and Figure 142. The aluminum is still characterized by a better performance.

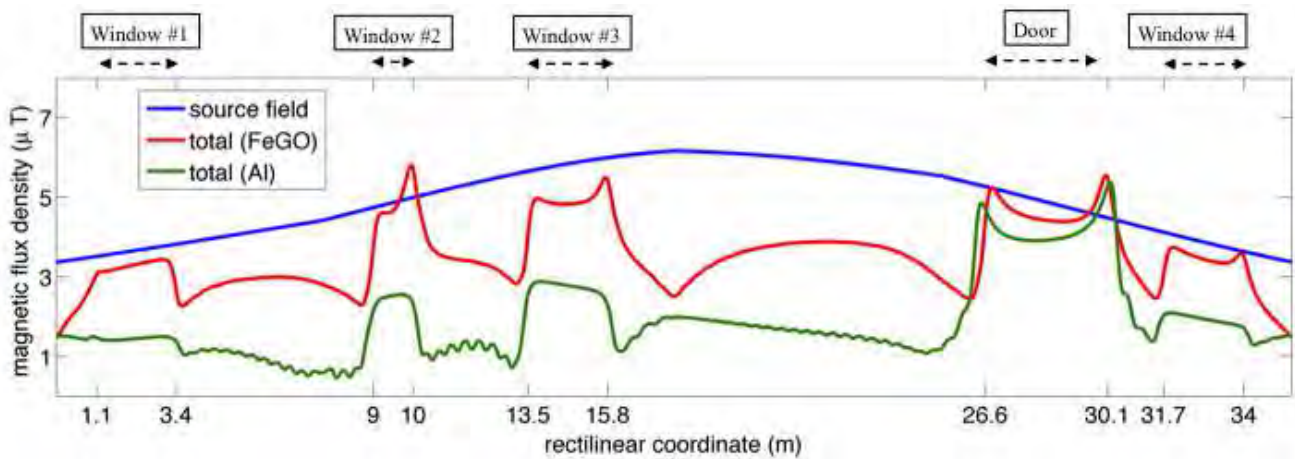Figure 140 – Magnetic flux density along the inspection line 1. With reference to Figure 1, the field is computed through the inspection line starting from the lowest corner and moving in counterclockwise direction. Therefore, the first hole that is encountered is window #1 and the last one is window #4
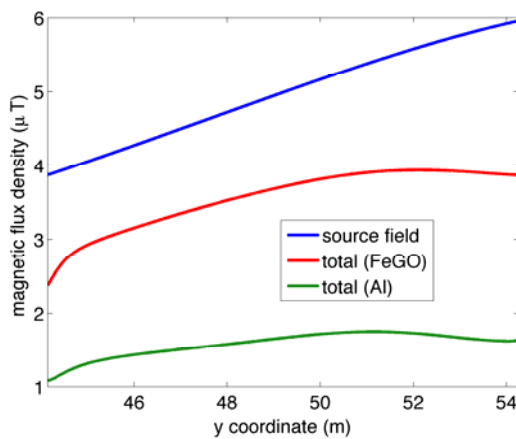

Figure 141 – Magnetic flux density along the inspection line 2.

Figure 142 – Magnetic flux density along the inspection line 3.

The analysis was performed trying to compare two solutions characterized by two different materials but with the total weight of the screening system and material costs very similar. In this case it is clear that aluminium solution is the best one. In general the conductive open shield work better of the ferromagnetic one.

In contrast, the ferromagnetic shields are easier to install because the shielding material is easily workable on the construction site and the union of the different laminates, that comprise the shielding system, can be performed with a simple overlap while in the case of the shielding purely conductive type is necessary welding as shown in Figure 143 where the images of the implementation of the shielding system described before are presented .

143

In the case of open shields in which are required shielding factor values relatively low ferromagnetic shields are preferable. Conversely, if the required SF are relatively high are always used solutions of conducting type.

Figure 143 – Pictures of the conductive shield during the realization of the system

6 References

[1] Review of the scientific evidence for limiting exposure to electromagnetic fields (0-300 ghz), Tech. Rep. Vol. 15 N.3, National Radiological Protection Board (2004).
URL www.nrpb.org [April 17, 2013]

[2] S. Kandel, Elf policies worldwide - protection of general public, WHO Workshop (June 2007).

[3] International Commission on Non-Ionizing Radiation Protection: http:/www.icnirp.de [April 17, 2013].

[4] ICNIRP, Guidelines for limiting exposure to time-varying electric, magnetic, and electromagnetic fields (up to 300 GHz), Health Phys 74 (4) (1998) 494–522.

[5] ICNIRP, Guidelines for limiting exposure to time-varying electric and magnetic fields (1 hz - 100 khz), Health Phys 99 (6) (2010) 818–836.

[6] ICNIRP, Guidance on determining compliance of exposure to pulsed and complex non-sinusoidal waveform below 100 kHz with icnirp guidelines, Health Phys 84 (3) (2003) 383–387.

[7] Directive 2004/40/ec of the european parliament and of the council of 29 april 2004 on the minimum health and safety requirements regarding the exposure of workers to the risks arising from physical agents(electromag- netic fields) (18th individual directive within the meaning of article 16 (1) of directive 89/391/eec) european parliament; council of the european union.

[8] Emf exposure standards applicable in europe and elsewhere, Tech. rep., Union of the Electricity Industry Eurelectric (March 2006).

[9] V. Rashkes, R. Lordan, Magnetic field reduction methods: efficiency and cost, IEEE Trans. Power Del. 13 (2) (1998) 552–559. doi:10.1109/61.660928.

[10] M. Reta-Hern´andez, G. G. Karady, Attenuation of low frequency magnetic fields using active shielding, Electr. Power Syst. Res. 45 (1998) 57–63.

[11] L. Ippolito, P. Siano, Using multi-objective optimal power flow for reducing magnetic fields from power lines, Electr. Power Syst. Res. 68 (2004) 93–101.

[12] I. Habiballah, A. Farag, M. Dawoud, A. Firoz, Underground cable magnetic field simulation and management using new design configurations, Electr. Power Syst. Res. 45 (1998) 141–148.

[13] A. Canova, D. Bavastro, F. Freschi, L. Giaccone, M. Repetto, Magnetic shielding solutions for the junction zone of high voltage underground power lines, Electr. Power Syst. Res. 89 (2012) 109–115.

[14] H. San Segundo, V. Roig, Reduction of low voltage power cables electromagnetic field emission in mv/lv substations, Electr. Power Syst. Res. 78 (2008) 1080–1088.

[15] G. Antonini, A. E. Ruehli, and J. Esch. "Nonorthogonal PEEC formulation for time and frequency domain modeling," IEEE International Symposium on Electromagnetic Compatibility, pp. 1:452–456, 2002.

[16] A. E. Ruehli, G. Antonini, J. Esch, J. Ekman, A. Mayo, and A. Orlandi. "Nonorthogonal PEEC formulation for time- and frequency-domain em and circuit modeling," IEEE Transactions on Electromagnetic Compatibility, pp. 45(2):167 – 176, 2003.

[17] O. Chadebec, J. Coulomb, J. Bongiraud, G. Cauffet, P. Le Thiec, Recent improvements for solving inverse magnetostatic problem applied to thin shells, IEEE Transaction on Magnetics 38 (2) (2002) 1005–1008.

[18] L. Giaccone, D. Ragusa, M. Khan, O. Manca, Fast magnetic field modeling for shielding systems, IEEE Transaction on Magnetics, in press.

[19] FEMM website: http://www.femm.info [April 17, 2013].

[20] Canova A, Freschi F, Repetto M, Tartaglia M. Description of power lines by equivalent source system. COMPEL 2005; 24:893–905.

[21] R. Turri, P. Casagrande, A. Canova, L. Giaccone, M. Manca Simplified power transformer models for environmental magnetic impact analysis. Paris : International Conference on Extremely Low Frequency Electric and Magnetic Fields, 2011. pp. 137-147.

[22] O. Bottauscio, M. Chiampi, D. Chiarabaglio, F. Fiorillo, L. Rocchino, M. Zucca, Role of magnetic materials in power frequency shielding: numerical analysis and experiments, in: IEE Procedings of Generation, Transmission and Distribution, Vol. 148, 2001, pp. 104–110.

[23] O. Bottauscio, M. Chiampi, D. Chiarabaglio, M. Zucca, Use of grainoriented materials in low-frequency magnetic shielding, J. Magn. Magn. Mater. 215-216 (2000) 130–132.

[24] Bavastro D., Canova A., Freschi F., Giaccone L., Manca M. (2013) *3D Modelling of Conductive and Ferromagnetic Shields.* In: International Council on Extremely Low Frequency Electric and Magnetic Fields, Nara, Japan, 14-18 October 2013. pp. 173-180

[25] F.Freschi, M.Repetto, A general framework for mixed structured/unstructured PEEC modelling, ACES J. 23 (3) (2008) 200–206.

[26] E. Tonti, "Finite formulation of electromagnetic field," IEEE Transactions on Magnetics, pp. 38:333–336, 2002.

[27] E. Tonti, "Finite formulation of the electromagnetic field," Progress in Electromagnetics Research, PIER 32 (Special Volume on Geometrical Methods for Computational Electromagnetics), 2001.

[28] Bavastro D., Canova A., Giaccone L., Manca .M (2013), Integral and analytical models for evaluating the distance of compliance, Int. J. Numer. Model., Doi: 10.1002/jnm.1941, in press.

[29] D. Bavastro, A. Canova , L. Giaccone (2011), *Multilayer shields for MV/LV electrical substations.* In: International Conference on Extremely Low Frequency Electric and Magnetic Fields, Paris (France), 24-25 March 2011. pp. 465-475

[30] Bavastro D., Canova A., Giaccone L., Manca M. (2013), "0" Emission MV/LV substation. In: International Council on Extremely Low Frequency Electric and Magnetic Fields, Nara, Japan, 14-18 October 2013. pp. 112-118

[31] Bavastro D., Canova A. , Giaccone L. , Manca M. (2013), *Mitigation of Complex MV/LV Substation.* In: International Council on Extremely Low Frequency Electric and Magnetic Fields, Nara, Japan, 14-18 October 2013. pp. 165-172

[32] O. Bottauscio, M. Chiampi, A. Manzin, Numerical analysis of magnetic shielding efficiency of multilayered screens, IEEE Trans. Magn. 40 (2) (2004) 726–720.

[33] A. Mager, Magnetic shield, IEEE Trans. Magn. 6 (1) (1970) 67–75.

[34] Y. Du, T. Cheng, A. Farag, Principles of power-frequency magnetic field shielding with flat sheets in a source of long conductors, IEEE Trans. Electromagn. Compat. 38 (3) (1996) 450–459. doi:10.1109/15.536075.